UNIVERSITY OF CALIFORNIA

Santa Barbara

The Holocene History and Facies Architecture of the Nueces Bayhead Delta of the Northwestern Gulf of Mexico

A Thesis submitted in partial satisfaction of the

requirements for the degree Masters of Science

in Geological Sciences

by

Johnathan Aaron Rice

Committee in charge:

Professor Alexander Simms, Chair

Professor Ed Keller

Professor David Lea

December 2015

The thesis of Johnathan Aaron Rice is approved.

_____

Ed Keller

_____

David Lea

_____

Alexander Simms, Committee Chair

December 2015

ACKNOWLEDGEMENTS

"He who asks is a fool for five minutes, but he who does not ask remains a fool forever."

-Mark Twain

Like many others, I would not be who I am or where I am today without the guidance and support and of many people. First, I would like to thank my mom and dad for their support in my pursuit of this path. Without their insight and experience I would not be where I am today. I would also like to thank my advisor, Alex, for allowing me to participate in this project, giving me the opportunity to discover the joy of research, and always having an open door for me to walk in. The Simms, lab group for getting muddy in the delta and collecting all the cores for this study as well as providing different perspectives while at UCSB. Lastly, the quote above was written on a plaque my dad had hanging in our kitchen growing up and has always been in the back of my mind, prompting me to always ask.

This research was funded in part by the Gulf Coast Association for Geologic Societies (GCAGS) Student Grant Program, the Ed Picou Fellowship Grant sponsored by the Gulf Coast section of the Society for Sedimentary Geology (SEPM) and the National Science Foundation (NSF), grant EAR-0921963.

ABSTRACT

The Holocene History and Facies Architecture of the Nueces Bayhead Delta of the Northwestern Gulf of Mexico

By

Johnathan Aaron Rice

The economic importance of coastlines highlights the need to understand how coasts evolve in response to changing climate. Prior work suggests that many of the estuaries in the northwestern Gulf of Mexico underwent large changes at 2.6, 4.8, and 8.2 ka. Twenty-eight vibracores, eight Geoprobe cores, twenty-eight radiocarbon ages, and twenty-five kilometers of seismic profiles were used to determine the response of the Nueces Bay-head Delta to the 2.6 ka and 4.8 ka events. Within the cores we identified nine sedimentary facies representing five distinct deltaic environments. Within the 25 kilometers of seismic data, we identified five seismic facies that correspond to the deltaic environments identified within the sediment cores.

Fifteen sand lobes interpreted to be buried mouth-bar deposits identified in the seismic profiles and cores were used to track changes in the location of the seaward edge of the delta through the middle to late Holocene. Following progradation of the delta at 6.9 ka, the delta underwent two back-stepping events in which the delta front transgressed up to 20 km at 4.8 ka and 2.6 ka. Following these two back-stepping events the delta prograded up to 14 km seaward of the maximum landward location of the delta. During delta progradation

from 4.8-3.2 ka, 11 ± 2.4 x10^3 m^3/yr of sand was delivered to the delta. During delta back-stepping from 3.2-2.6 ka, 5.9 ± 2.4 x10^3 m^3/yr of sand was delivered to the delta. During the last phase of delta progradation from 2.6 ka-present, 5.3 ± 2.4 x10^3 m^3/yr of sand was delivered to the delta. The decrease in the volume of sand delivered to the delta during the back-stepping event at a time when the rate of sea-level rise was decreasing and regional records of climate show drying suggests that the back-stepping events were likely driven by climate changes.

TABLE OF CONTENTS

LIST OF FIGURES

Introduction

Approximately 40% of the global population lives within 100 km of the coast (CIESIN, 2013). These coastal systems are threatened by natural climate change and anthropogenic activities (Wallace et al., 2009). Most studies examining the future fate of coastlines in response to anticipated climate change focus on the impacts of increased sea-level rise (Pethick, 2001; Church and White, 2006; FitzGerald et al., 2008). However, other factors associated with climate change, including diminished sediment supply to coastal systems, may also provide a mechanism for triggering rapid coastline changes. The Holocene was marked by several periods of climate change both globally (Obrien et al., 1995; Mayewski et al., 2004) and across the northwestern Gulf of Mexico (Buzas-Stephens et al., 2014; Livsey et al., *In Review*). We hypothesize that the entire Nueces Delta underwent a rapid landward retreat (back-stepping) during periods of increased aridity. Back-stepping events at 2.6 ka and 4.8 ka reached a maximum transgression of 15 km (Simms et al., 2008). Coastal changes are commonly associated with relative sea-level change in response to climate change. However, recent regional sea-level curves (Simms et al., 2007; Törnqvist et al., 2004; Livsey and Simms, 2013) suggest that sea levels at 2.6 ka and 4.8 ka did not experience a steep increase in the rate of rise but were gradually decreasing. Seaward edges of bayhead deltas are generally stable when the sediment supply is balanced with the rate of sea-level rise and ocean dispersal patterns (Nichols, 1989, Yang et al., 2003). During droughts, sediment supply to bayhead deltas decrease due to lower stream discharge (Rodriguez et al., 2000; Fraticelli, 2006). Diminished sediment supply during drought may cause the front of bayhead deltas to retrograde.

The purpose of this study is to examine the response of the Nueces Delta to Holocene climate changes. Sediment cores and high-resolution seismic profiles were used to map the location of the bayhead delta over the last 8 ka. Combined with radiocarbon ages and grain-size data quantifying the amount of sand delivered to the delta, we document the history of the delta. In addition to documenting the history and evolution of the Nueces Delta, this study provides additional insights into the understanding of bayhead-delta architecture.

Background

Study Area

The Nueces Bay/Corpus Christi Bay system is located along the central Texas coast within the northwestern Gulf of Mexico (Fig. 1A). The Nueces River flows into the upper reaches of Nueces Bay forming a bayhead delta (Fig. 1B). The Nueces River begins in the Edwards Plateau of central Texas and generally flows south towards the Gulf of Mexico over a course of approximately 507 kilometers (TCEQ, 2013). The drainage basin of the Nueces River covers an area of approximately 43,900 km^2 (TCEQ, 2013). The Nueces River supplies most of the freshwater and fluvial sediment to the Nueces Bay/Corpus Christi Bay system and is confined by the Nueces Incised Valley. The Nueces River is dammed at multiple locations. The most seaward dam is located approximately 20 km upstream from Nueces Bay and has reduced freshwater and fluvially derived sediment supply to the Nueces Bayhead Delta (Mannino and Montagna, 1996).

The tidal range of Nueces Bay is < 0.3 m (USGS, 2014). The maximum landward extent of tidal inundation is marked locally by an escarpment that extends from one side of the incised valley to the other and separates the lower delta-plain from the upper delta-plain (Fig. 2). Corpus Christi Bay is separated from the Gulf of Mexico by Mustang Island and

Nueces Bay is separated from Corpus Christi Bay by two spits (Fig. 1B). Tidal connectivity between the estuary and the Gulf of Mexico occurs through Aransas Pass.

The Nueces Bay/Corpus Christi Bay system, from the delta to the barrier island, comprises a classic tripartite wave-dominated estuary system (Dalrymple et al., 1992). Currently, active sand deposition is occurring at the mouth of the Nueces River where the modern mouth bar is forming along the southern flank of the incised valley (Figs. 1C & 2). The rest of the delta receives sediment primarily during large river floods and during intermittent marine flooding (White et al., 2002).

Climate

Nueces Bay experiences a sub-humid to semi-arid climate with increasingly drier conditions upstream within the drainage basin of the Nueces River. Average annual rainfall within the delta is approximately 76 cm/year with an evaporation rate of approximately 145 cm/year (USGS, 2014).

Multiple global climate events have occurred at the millennial scale throughout the Holocene (Bond et al., 2001; Noren et al., 2002; Mayewski et al., 2004). During the early to middle Holocene, most of North America (Dean et al., 1996) and southwestern regions of Mexico (Bernal et al., 2011) experienced periods of aridity. The Edwards plateau, within the headwaters of the Nueces River in central Texas, experienced arid conditions that reached their peak from 2.5-5 ka (Blum and Valastro, 1989; Toomey et al., 1993; Blum et al., 1994). Leading up to, during, and following this peak aridity, the northwest Gulf of Mexico experienced intermittent millennial-scale shifts between wetter and drier climate conditions (Poore et al., 2003; Buzas-Stephens et al., 2014). The estuaries of the northwest Gulf of Mexico have experienced changes at similar frequencies, in particular at 2.6 and 4.8 ka.

(Anderson et al., 2008; Rodriguez et al., 2008; Simms et al., 2008; Simms et al., 2010; Troiani et al., 2011; Anderson et al., 2014).

Sea Level

During the last glacial maximum, 20 ka, sea level along the northwestern Gulf of Mexico was 90-100 m lower than present (Simms et al., 2007). The early Holocene rise in sea level was rapid until 6-7 ka at which point it reached 5-10 m below present-day sea level (Törnqvist et al., 2004; Simms et al., 2007; Simms et al., 2008; Milliken et al., 2008; Rodriguez et al., 2010). The Gulf of Mexico has experienced a relatively steady decrease in the rate of sea-level rise over the past 6-7 ka (Simms et al., 2008, Livsey and Simms, 2013) with an average rate of 0.4 to 0.6 mm/yr over the last 4 ka (Milliken et al., 2008).

Methods

Core Collection and Seismic Acquisition

Six geoprobe cores and twenty-nine vibracores were collected during the summer of 2012 (Fig. 1C). Two additional geoprobe cores were collected in the summer of 2008. Cores range from three to fifteen meters in length. All cores were split and described at the sedimentology and stratigraphy lab at the University of California, Santa Barbara. The vibracores collected on the seaward edge of the Nueces Delta were used to establish the sedimentary characteristics of facies observed within the delta and better interpret longer cores (Figs. 3 & 4). Additionally, twenty-five kilometers of seismic data (Fig. 1C) was collected from upper Nueces Bay and within the distributary channels of the Nueces Delta with an Edgetech SB-216S full spectrum sub-bottom profiler operated using an Edgetech 3200XS topside unit. The seismic data was processed using a standard band pass filter and

automatic gain control. A time-depth conversion was made using a velocity of 1580 m/s (Simms et al. 2008)

Coarse Fraction

Coarse fraction analysis was used to aid in interpreting depositional environments based on a modified version of the Shepard and Moore (1954) method. Samples were sieved using a 63 μm sieve to isolate the coarse fraction. Minerals, plant material, shell material, foraminifera, ostracods, insects, and charcoal were counted and their relative abundances determined.

Grain Size

Grain-size analysis was performed on nine of the sediment cores (Figs. 1C & 5) using a CILAS 1190 laser particle size analyzer. Five geoprobe cores with lengths ranging from 6.1 – 12.2 m were sampled at 10 cm intervals and four vibracores with lengths ranging from 1.4 – 4 m were sampled at 20 cm intervals. All grain-size analysis samples were pre-treated using 30% hydrogen peroxide (H_2O_2) to remove organics and 10% hydrochloric acid to remove carbonates (Kirby et at., 2014).

Radiocarbon Dating

Twenty eight accelerated mass spectrometry radiocarbon ages (Table 1) were obtained from articulated and non-articulated bivalves, gastropods, foraminifera, a crustacean pincer, and a piece of wood. The global marine carbon reservoir is 440 years (Stuvier et al., 1998); however, fluvial derived "dead" carbon can bias ages when using bivalves. Radiocarbon reservoir effects are commonly corrected for by using the difference in age between organic material (charcoal or plant material) and marine carbonate deposited concurrently (Aten, 1983). Simms et al. (2008) dated a piece of wood and a barnacle attached

to it within Corpus Christi Bay. The difference between the wood and the barnacle was 760 years before the dates were calibrated, suggesting a local radiocarbon reservoir of 760 years within Corpus Christi Bay. We estimated the local radiocarbon reservoir effect within Nueces Bay using a similar method. An articulated bivalve (*Macoma tageliformis*) was sampled at a depth of 703 cm in core ND12-18 (Fig. 4). A piece of wood was also sampled at the same depth as the bivalve and both materials were dated. The difference in age was used as the radiocarbon reservoir for all ages except for one obtained from an unidentified terrestrial gastropod from core ND12-17. All ages were calibrated using the Marine13 curve (Reimer et al., 2013) in CALIB v7.0.2 except for the unidentified gastropod, which was calibrated using the IntCal13 curve (Reimer et al., 2013).

Sediment Supply Calculations

We used the volume of sand as a conservative record of sediment supply to the delta due to the potential of finer-grained material to be exported from the bay (Shideler et al., 1984). Sand supply was determined by multiplying the percent sand for each facies by the total sediment volume stored in the delta through time. Sediment supply, as measured in volume, was calculated by subtracting the elevations of stratigraphic surfaces identified within sediment cores and seismic profiles. Five main surfaces were used for the volumetric calculations. The lowest surface was constructed from the contour map of the Nueces Incised Valley from the study of Simms et al. (2008). The original incised valley contours extend from the seaward edge of the delta to Mustang Island. We extended those contours landward using a Pleistocene contact in core ND12-17 as well as channel sand deposits observed in the bottom of cores ND12-18 and 12-20. Two incised valley surfaces were created to account for errors associated with this extrapolation. One surface assumes the incised valley is v-shaped

and the other surface assumes the incised valley is u-shaped thus establishing a minimum and maximum estimate respectively. Four overlying surfaces were constructed based on stratigraphic surfaces identified in sediment cores. The upper-most surface is the modern topography and bathymetry obtained from a digital elevation model from NOAA (2008).

The sediment volume supplied to the delta (V_a) (Table 2) was determined by averaging the maximum (using a U-shaped valley) and minimum (using a V-shaped valley) sediment volume scenarios according to the following equation:

$$V_a = ((U_u - U_l) + (V_u - V_l))/2$$

where U_u is the volume of the U-shaped valley below the upper surface, U_l is the volume of the U-shaped valley below the lower surface, V_u is the volume of the V-shaped valley below the upper surface, and V_l is the volume of the V-shaped valley below the lower surface. The sand supply (V_s) was determined by multiplying V_a by the sand percentages of each of the respective environments (Fig. 5) in the following manner:

$$V_s = (((V_a * M)) * S_m) + (((V_a * LDP)) * S_{ldp})$$

where M is the percent of the valley filled during that time interval with mouth bar deposits, S_m is the average sand content of the mouth bar deposits, LDP is the percent of the valley filled during that time interval with lower-delta plain deposits, and S_{ldp} is the average sand content of the lower-delta plain deposits.

The total error (E_t) was determined in the following manner:

$$E_t = ((E_v^2) + (E_s^2))^{1/2}$$

where E_v is the difference in sand content between the maximum sediment volume and the average sediment volume and E_s is the difference between V_s and V_s calculated using one standard deviation higher than the mean of the S_m and S_{ldp} distributions.

Results

Sedimentary Facies

Nine sedimentary facies were identified in the cores (Fig. 6).

Mud Facies 1

The uppermost facies observed in the lower delta-plain is Mud-facies 1 (M1) (Fig. 6). M1 is a mottled grey clayey silt with little to no shell material. This facies has burrows filled with sandy silt. Modern root fragments are found in the top of cores sampling this facies. Shell material increases with depth from 0% to a maximum of 5% in the bottom 20 cm of this facies. When present, shell material consists of *Mulinia sp.* and *Rangia sp.* Gastropod shell fragments were also present but too fragmented to identify. The overall thickness of the beds of this facies ranges from 90 to 130 cm.

Mud Facies 2

Mud facies 2 (M2) (Fig. 6) is dominantly composed of silt (>80%) with little to no sand. M2 is characterized by laminated beds of light and dark grey muds. No plant material or shell material was observed in this facies.

Mud Facies3

Mud Facies 3 (M3) (Fig. 6) is a black/dark gray mud with less than 15% sand. No shell material is observed in M3. However, organic material, such as roots or other plant fragments are commonly present. M3 is observed within the upper 50 centimeters of all of the Geoprobe cores taken on the upper-delta plain. M3 is commonly overprinted with pedogenic features such as calcium carbonate nodules and capped by a distinct organic-rich horizon.

Sand Facies 1

Sand Facies 1 (S1) (Fig. 6) is a structureless sand with clayey silt-filled burrows and shell fragments. S1 contains >40% sand by volume but some samples contained over 80% sand. Shell fragment content ranges from 5-20% by volume and is composed of *Mulinia sp.*, *Rangia flexuosa*, *Macoma tageliformis*, and *Crassostrea virginica*. *Crassostrea virginica* is highly fragmented when observed and never found articulated. Gastropod shell fragments were also observed but too fragmented for identification. S1 underlies M1 in most cores (Fig. 2). The contact between these two facies is usually sharp but a gradational contact, composed of a fining up sequence between the two faces, is observed in two cores. Beds of S1 range in thickness from 1 to 1.5 m.

Sand Facies 2

Sand Facies 2 (S2) (Fig. 6) is composed of mottled grey and brown silty sand (60% sand) with approximately 15% shell fragments by volume. Plant and root material is observed within the facies as well as non-articulated fragments of *Rangia flexuosa*.

Sand Facies 3

Sand facies 3 (S3) (Fig. 6) is a poorly sorted, sub-rounded to rounded, fine to medium sand. S3 is brown and devoid of any shell material or organics.

Sand Facies 4

Sand Facies 4 (S4) (Fig. 6) is composed of tan rounded, very fine sand with less than 15% silt. No shell material or organics were observed in S4 but large calcium carbonate nodules with exsolution rims were observed.

Oyster Facies

An oyster-rich mud or sand (Fig. 6) was found in cores ND12-05 and ND12-09 (Appendix B) obtained from the seaward edge of the Nueces Delta. This facies is composed

of articulated clusters of *Crassostrea virginica* shells within a silty or sandy matrix (Fig. 5). The oyster shells range from 3-7 cm in length. Other shell fragments are found within the oyster facies including *Mulinia sp.*, *Rangia flexuosa*, and *Macoma tageliformis.*

Shell-Hash Facies

The shell-hash facies (SH) (Fig. 6) is composed of >80% shell fragments by volume. The shell fragments range in size from 0.5-2 cm. No articulated bivalves were found in the shell-hash facies but the valves observed ranged from entirely intact to small shell fragments. The shell-hash facies is found in association with the oyster facies.

Seismic Facies

Seismic data was collected in the bay, along two distributaries within the delta and along the main stem of the Nueces River (Fig. 1C). Five distinct facies were identified (Fig. 7)

Seismic Facies 1

Seismic facies 1 (SE1) is characterized by high amplitude, closely spaced, parallel reflections. (Fig. 7)

Seismic Facies 2

Seismic Facies 2 (SE2) is characterized by chaotic to transparent reflections. SE2 is commonly bound by a high amplitude reflection (Fig. 7).

Seismic Facies 3

Seismic Facies 3 (SE3) is composed of a series of dipping, en echelon reflections. SE3 is commonly bound by a horizontal high amplitude reflection (Fig. 7). SE3 has a similar geometry as the parallel prograding clinoforms of Mitchum et al., (1977).

Seismic Facies 4

Seismic Facies 4 (SE4) is composed of sets of complex sigmoid oblique reflections (Mitchum et al., 1977) (Fig. 7).

Seismic Facies 5

Seismic Facies 5 (SE5) is composed of lower amplitude reflections similar to the prograded fill of Mitchum et al., (1977) (Fig. 7). SE5 is commonly bound by a high amplitude reflection.

Coarse Fraction

Coarse Fraction analysis was performed on twenty-three samples from the lower-delta plain, mouth bar and upper-bay environments. Sixteen of the twenty-three samples were obtained from the upper five centimeters of sediment cores and the other seven samples were sampled at depths ranging from 15-60 cm, beneath facies contacts. The purpose of employing coarse fraction analysis was to distinguish lower-delta plain sediments from upper-bay sediments. While one comparison proved promising (Fig. 8), no major distinction was found within the coarse fraction to distinguish upper-bay sediments from lower delta-plain sediments. The inability to distinguish upper-bay sediments from lower delta plain sediments may be attributed to the variety of sedimentary regimes experienced within the lower delta plain including marine, intermittent marine, and fluvial. Lower-delta plain sediments deposited by intermittent sub-marine or fluvial processes may be distinguished from upper-bay sediments based on their lower abundances of foraminifera or plant material. However, tidal distributaries also comprise a large portion of the lower-delta plain and exhibit similar sedimentary characteristics as upper-bay sediments. As such, sediments deposited landward of the shoreline in tidal distributaries contain similar flora and fauna abundances as upper-bay deposits and the two sedimentary deposits are indistinguishable.

Radiocarbon Ages

Twenty-eight radiocarbon ages were obtained from the sediment cores (Table 1). A difference of 365 years was found between a paired articulated bivalve and a piece of wood sampled at the same depth in core ND12-18 (Fig. 4). The difference of 365 years was used as the local radiocarbon reservoir for all ages except for the unidentified terrestrial gastropod.

Sand Supply

Sand supply was calculated over three periods of time from approximately 4.8 ka-3.2 ka, 3.2 ka-2.6 ka, and 2.6 ka-present. From 4.8-3.2 ka, $11 \pm 2.4 \times 10^3$ m^3/yr of sand was delivered to the delta. From 3.2-2.6 ka $5.9 \pm 2.4 \times 10^3$ m^3/yr of sand was delivered to the delta. From 2.6 ka to present, $5.3 \pm 1.1 \times 10^3$ m^3/yr of sand was delivered to the delta.

Discussion

Facies Interpretations

The nine sedimentary facies and five seismic facies identified in this study were grouped into five major depositional environments (Fig. 2) (Table 3). The five major depositional environments were used to reconstruct the middle to late Holocene evolution of the Nueces Bayhead Delta (Fig. 9). These environments include mouth bar, lower-delta plain, upper-delta plain, upper bay, and fluvial.

Mouth Bar

Sand facies 1 (S1) (Fig. 6) (Table 3) is interpreted to represent mouth bar deposits based on its sandy, well-sorted nature. *Rangia flexuosa* and *Mulinia lateralis* were sampled in the modern mouth bar and in S1 in cores. No structures were observed in either the modern mouth bar deposit or where S1 was observed in sediment cores. The absence of structures in S1 may be attributed to either disturbance during sampling and/or bioturbation.

Three articulated bivalves of approximately the same age were obtained from a three meter thick bed of S1 in core ND12-23 (Figs. 3 & 4) suggesting that beds of S1 were deposited rapidly, consistent with a mouth bar interpretation. Seismic facies 2 (SE2) is also interpreted as mouth bar deposits based on its chaotic nature suggesting a sandy character to the deposits and the character of sediments within sampled intervals of a similar seismic facies by Simms et al., (2008). Seismic facies 3 (SE3) (Fig. 7) exhibits a progradational geometry expressed as parallel prograding clinoforms (Mitchum et al., 1977). This facies likely also represents the mouth bar as it prograded during a period of higher sediment supply.

Lower-Delta Plain

Deposition within the modern lower delta plain is controlled primarily by intermittent marine processes (Olariu and Bhattacharya, 2006). Mud facies 1 (M1) and Mud facies 2 (M2) (Fig. 6) (Table 3) are interpreted to represent lower-delta- plain deposits based on the scarcity or absence of shell material, little to no soil development, and their occurrence in the tops of cores from the modern lower-delta-plain. M1 represents the portion of the lower-delta plain that is intermittently exposed and experiences intermittent deposition from tide, wind-wave, and fluvial processes. The modern extent of M1 deposits on the surface of the delta is confined by the incised valley to the north, the Nueces River to the south, the bay to the east, and an erosional scarp to the west. M2 was observed in a core collected in a tidal channel within the Nueces Bayhead Delta. Thus M2 likely represents the tidal distributary network commonly associated with deltas (Olariu and Bhattacharya, 2006).

Upper-Delta Plain

Mud Facies 3 (M3) (Fig. 6) (Table 3) is interpreted to represent deposits from the upper-delta plain based on its finer grained nature, the presence of roots and other organic

material and the absence of shell material. It also occurs in the tops of cores from the upper-delta plain. The upper-delta plain experiences less periods of sub-aqueous deposition compared to the lower-delta plain except during large floods or storm surges. Pedogenic processes have overprinted most occurrences of M3. Soil horizons are well developed with O, A, E, and B horizons present. Calcium carbonate nodules were observed in all M3 deposits.

Upper Bay

Due to only one core (ND12-08) sampling upper-bay sediments (Fig. 8) in this study, we relied on the descriptions of upper-bay sediments by Simms et al., (2008) to identify this facies. However, seismic profiles did image what were interpreted as upper-bay deposits (SE1). This interpretation is based on the presence of seismic facies 1 (SE1) in the upper portion of seismic profiles collected from the upper bay of Nueces Bay. (Fig. 7)

Oyster facies (OF) (Fig. 6) (Table 3) is interpreted as an oyster reef. Oyster reefs are common in the bay today and occur within upper and open bays throughout the northwestern Gulf of Mexico (Buroker, 1983). *Crassostrea virginica* sampled in OF are the same species observed in modern oyster reefs. A distribution of species commonly found with modern oyster reefs was also observed in OF including *Mulinia sp., Rangia flexuosa,* and *Macoma tageliformis*. Shell hash facies (SF) is interpreted as distal oyster reef deposits based on its location conformably on top of OF in cores as well as the broken nature of the shell material in SF.

Fluvial Facies

Sand Facies 2 (S2) (Fig. 6) (Table 3) is interpreted as a levee deposit. The interpretation of S2 is based on the interbedded nature of the brown and grey deposits and its

presence in core tops from cores collected on the modern levee. Sand facies 3 (S3) is poorly sorted and composed of fine to coarse sand. S3 is brown, devoid of any shell material or organics and was only observed in the deepest sections of two Geoprobe cores. S3 is interpreted as channel sands based on its poor sorting, low clay/silt content, and the absence of shell material. Sand facies 4 (S4) is interpreted as Pleistocene fluvial terrace deposits based on the absence of organic material and the presence of large (1-3 cm) calcium carbonate nodules with exsolution rims.

Seismic facies 4 (SE4) is interpreted as a point bar deposit. Both SE3 and SE4 (Fig. 7) contain oblique reflections. However, SE4 was interpreted as a fluvial facies because the complex sigmoid oblique reflections within SE4 lead laterally into a channel-like geometry. While the parallel prograding clinoforms of SE3 grade distally into horizontal reflections. Seismic facies 5 (SE5) is interpreted as channel fill based its geometry (Fig. 7).

Facies Architecture

Deltas commonly exhibit well defined topsets and foresets (Gilbert, 1885). However, accommodation plays an important role in the development of foresets within deltas and thus the foresets are not ubiquitous within all deltas (Milligan and Lemons, 1998). Such deltas lacking foresets have been referred to as topset-dominated deltas (Edmonds et al., 2011). The Nueces Delta, similar to other bayhead deltas within the Gulf of Mexico, is topset dominated (Edmonds et al., 2011). The topset nature and poorly-developed to absent pro-delta environment during the middle and recent Holocene is likely due to the shallow water depth characteristic of Nueces Bay.

Another characteristic feature of the Nueces Bayhead Delta is the nature of the mouth bar deposits. Deposition of the mouth bar sands within the delta is episodic in nature. Most

mouth bar deposits are composed of 1-2 m thick beds. Radiocarbon ages from the top and bottom of these beds are essentially the same age (Fig. 3). Although deposition occurred rapidly, each mouth bar package is geographically isolated similar to the deltaic overbank deposits of Shen et al., (2015). While the modern mouth bar is found in a water depth of 1-2 m and most mouth bar deposits sampled in this study are less than 3 m, a 6.9 ka mouth bar deposit located in core ND12-18 (Fig. 4) is approximately 6 m thick, which is thicker than any other mouth bar deposits sampled. The thicker mouth bar at 6.9 ka may be attributed to greater accommodation as sea-level was rising faster at 6.9 ka (Simms et al., 2007; Milliken et al., 2008). Some of this greater accommodation may have been a direct result of the 0.4-2 m of rapid sea-level rise at 8.2 ka (Törnqvist et al., 2004; Kendall et al., 2008; Rodriguez et al., 2010).

Bedload deposition within the delta is focused at the mouth bar. However, most of the suspended load is carried out into the bay. Within Corpus Christi Bay, wind resuspension is an important process for clay sized sediments (Shideler, 1984). One ubiquitous feature within the Nueces Bayhead Delta system is the large and thick accumulation of muddy lower-delta plain deposits flanking the much smaller sandy mouth bars. This “mud plug” currently to the north of the modern mouth bar constitutes an important component of the Nueces Incised Valley fill. The “mud plug” is likely sourced from overbank deposition during fluvial flooding from the Nueces River as well as a component of re-suspended muds brought onto the lower delta plain by the wind waves and tides (Shideler, 1984; White et al., 2002). Similar “mud plugs” may be an important yet unrecognized portion of incised valley fills.

Deltaic Evolution

Radiocarbon ages obtained from this study and a previous study (Simms et al., 2008) were used to reconstruct the evolution of the delta through the Holocene. The locations of mouth bars interpreted from Sand Facies 1 and Seismic Facies 2 in conjunction with paleo-bayhead delta deposits dated and documented by Simms et al., (2008) record the back-stepping and prograding of the delta through time (Fig. 9).

The only deposits older than 8.2 ka sampled in this study were deposits from fluvial facies in three cores approximately 11 km from the mouth of the Nueces River. Sand facies 4 (S4) in core ND12-17 is interpreted as a Pleistocene terrace deposit (Figs. 4 & 6). Sand facies 3 (S3) interpreted as channel sand deposits and observed in cores ND12-18 and ND12-20 (Figs. 4 & 6) may not be contemporaneous, but both are overlain by similarly aged lower-delta plain deposits. These fluvial deposits likely fed a delta identified approximately 8 km seaward of the modern mouth bar by Simms et al. (2008). The mouth bar identified by Simms et al., (2008) near the modern Rincon Point (Fig. 10C) marks the farthest seaward position of the delta from 8.2 ka to the present.

Following rapid transgression at 8.2 ka (Kendall et al., 2008; Simms et al., 2008; Rodriguez et al., 2010), the delta transgressed approximately 20 km from Rincon Point to core ND12-18. During this retreat the delta stabilized periodically forming three seismically identified mouth-bar deposits 12 km west of Rincon Point sometime before 6.9 ka but after 8.2 ka. The three seismically identified mouth bars are assigned to this age based on their elevation of 12-14 mbsl and their position in the incised valley. Also, during this retreat the delta passed through core ND12-25 approximately 15 km west of Rincon Point at 6.9 ka. The transgression from 8.2 – 6.8 ka represents flooding surface 1 (FS1). Following the transgression that formed FS1, the delta mouth bar prograded east up to 20 km from core

ND12-18 at 6.9 ka to Rincon Point at 5.0 ka. During this time period the delta mouth bar passed through core NB03-02 at 5.6 ka.

Following the progradation culminating at 5.0 ka, the delta mouth bar backstepped 22 km from Rincon Point to core ND08-02 at 4.5 ka (Fig. 10). During this transgression, the delta mouth bar passed through core ND12-25 at 4.6 ka approximately 15 km west of Rincon point. Similarly aged delta mouth bar deposits were identified in cores ND08-01 and ND08-02. This suggests the delta mouth bar was being deposited at ND08-01, 19 km from Rincon Point, and ND08-02, 22 km from Rincon Point, at 4.4 ka. The transgression from 5 ka to 4.5 ka represents flooding surface 2 (FS2). Following the transgression that created FS2, the delta mouth bar may have prograded 22 km from core ND08-02 at 4.5 ka to Rincon Point at 3.2 ka. The maximum regression at 3.2 ka at Rincon Point is based on an age from a bayhead delta deposit identified by Simms et al. (2008). However, No sediment cores or seismic profiles sampled any intermediary delta mouth bars that can be temporally associated with this regression. Seismic facies 2 (SE2), interpreted as a mouth bar, was identified in a profile older than 3 ka but may be younger than 3.2 ka. The seismically identified mouth bar suggests the delta mouth bar stabilized between core ND08-02 and Rincon Point. Thus a minimum regression halfway between core ND08-02 and Rincon Point is assumed to have occurred during this time.

Following the regression at 3.2 ka, the delta backstepped 6 – 18 km from Rincon Point to core ND12-20 at 2.5 ka (Fig. 10B). The delta mouth bar passed through core ND12-23 at 3 ka, 12 km west of Rincon Point, and passed through core ND12-12 at 2.8 ka, 15 km west of Rincon Point, before reaching core ND12-20 at 2.5 ka. The transgression from 3.2 ka

to 2.5 ka represents flooding surface 3 (FS3). Following FS3, the delta mouth bar prograded 10 km from core ND12-20 to its modern position passing through core ND12-11 at 2 ka.

Correlation with Paleoclimate Records

A recent study of foraminiferal assemblages within Baffin Bay located approximately 60 km to the south of the Nueces Bayhead Delta provides a centennial-scale record of climatic changes throughout the region (Buzas-Stephens et al., 2014). *Ammonia spp*. is the most abundant genera of foram in the Baffin Bay record and its abundance tracks changes from xeric to more mesic climates. The transgression and regression of the Nueces Bayhead Delta follows the proportion of *Ammonia spp.* through time (Fig. 10). Maximum landward transgression of the system occurred during periods of maximum arid conditions. Similarly, upon the return of more mesic conditions, the bayhead delta prograded. These transgressions and regressions occurred at a time period when the rate of sea-level rise was decreasing, suggesting a dominant control of climate on the behavior of the delta.

Sand supply to the system mirrored the regressive and transgressive patterns of the Nueces Bayhead Delta from 4.8-3.2 ka and 3.2-2.6 ka respectively. Sand delivered to the delta was greater during the regression ($11 \pm 2.4 \times 10^3$ m^3/yr) than the transgression (5.9 ± 2.4 $\times 10^3$ km^3/yr). A decrease in sand supply during the transgression supports climate as the dominant driver of delta back-stepping from 3.2-2.6 ka. The post 2.6 ka regression was not was not marked by a return to higher sand supplies. However, the calculation of the post 2.6 ka sand supply is averaged over a longer time period and may mask higher frequency changes in sand supply.

Conclusion

This study identified nine sedimentary facies and five seismic facies defining five major depositional environments. The position and age of these deposits was used to illustrate how the Nueces Bayhead Delta migrated through the Holocene. Following the 8.2 ka event, the delta was located at a lower elevation and more seaward of its modern position. At 8.2 ka the delta backstepped at least 20 km with two other transgressive events occurring at 2.6 and 4.8 ka. The delta's position changed by up to 20 km during these two latter back-stepping events. The timing of these transgressive events correlates with periods of aridity across the northwestern Gulf of Mexico. In conjunction with the 2.6 ka back-stepping event, this period of aridity was marked by a decrease in the sand supplied to the delta suggesting climate was the dominant driver of the Holocene transgressive events within the delta.

References

Anderson, J.B., Rodriguez, A.B., Milliken, K.T. and Taviani, M. (2008) The Holocene evolution of the Gavleston estuary complex, Texas: evidence for rapid change in estuarine environments. In: Response of Upper Gulf Coast Estuaries to Holocene Climate Change and Sea-Level Rise (Eds J.B. Anderson and A.B. Rodriguez), Geol. Soc. Am. Spec. Pap., 443, 89–104, Boulder, CO.

Anderson, J.B., Davin J. Wallace, Alexander R. Simms, Antonio B. Rodriguez, Kristy T. Milliken. 2014. Variable response of coastal environments of the northwestern Gulf of Mexico to sea-level rise and climate change: Implications for future change Marine Geology. v. 352. p. 348-366

Aten, L.E. 1983. Indians of the Upper Texas Coast. Academic Press, New York, p. 370

Bernal, Juan Pablo, Matthew Lachinet, Malcolm McCulloch, Graham Mortimer, Pedro Morales, Edith Cienfuegos. 2011. A speleothem record of Holocene climate variability from southwestern Mexico. Quaternary Research. v. 75 p. 104-113

Bond, Gerard, Berard Kromer, Juerg Beer, Raimund Muscheler, Michael N Evans, William Showers, Sharon Hoffman, Rusty Lotti-Bond, Irka Hajadas, Georges Bonani. Persistent Solar Influence on North Atlantic Climate During the Holocene. Science. v. 294 p. 2130-2136

Blum Michael and Salvatore Valastro Jr. 1989. Response of the Pedernales River of Central Texas to Late Holocene Climate Change. Annals of the Association of American Geographers. v. 79. p.435-456

Blum, Michael D., Rickard S. Toomey III, Slavatore Valastro Jr. 1994. Fluvial response to Late Quaternary climatic and environmental change, Edwards Plateau, Texas. Paleogeography, Paleoclimatology, Plaeoecology. v. 108, p. 1-21

Buroker, N.E., 1983. Population genetics of the American oyster *Crassostrea virginica* along the Atlantic coast and the Gulf of Mexico. Marine Biology. v. 75 p. 99-112

Buzas-Stephens, Pamela, Daniel N. Livsey, Alexander R. Simms, Martin A. Buzas. 2014. Estuarine foraminifera record Holocene stratigraphic changes and Holocene climate changes in ENSO and the North American monsoon: Baffin Bay, Texas. Palaeogeography, Palaeoclimatology, Palaeoecology. v. 404, p. 44-56

Center for International Earth Science Information Network at Columbia University (CIESIN). 2013. Percentage of Total Population Living in Coastal Areas. http://sedac.ciesin.columbia.edu/es/papers /Coastal_ Zone_Pop_Method.pdf.

Church, John A. and Neil J. White. 2006. A 20th Century Acceleration in Global Sea-Level Rise. Geophysical Research Letters. v. 33, L01602, doi:10.1029/2005GL024826.

Dalrymple, Robert W., Brian A. Zaitlin, and Ron Boyd. 1992. Estuarine Facies Models: Conceptual Basis and Stratigraphic Implications. Journal of Sedimentary Petrology. v. 62, no. 6, p. 1130-1146.

FitzGerald, Duncan M., Michael S. Fenster, Britt A. Argow, and Ilya V. Buynevich. 2008. Coastal Impacts Due to Sea-Level Rise. Annu. Rev. Earth Planet Sci. v. 36, p. 601-647.

Fraticelli, Carmen. 2006 Climate Forcing in a Wave-Dominated Delta: The Effects of Drought-Flood Cycles on Delta Progradation. Journal of Sedimentary Research. v. 76, o, 1067-1076

Kendall, Roblyn A., Jerry X. Mitrovica, Glenn Al Milne, Torbjörn E. Törnqvist, Yongxiang Li. 2008. The sea-level fingerprint of the 8.2 ka climate event. Geology. v.36, no. 5, p. 423-426

Livsey, Daniel and Alexander R. Simms. 2013. Holocene sea-level change derived from microbial mats. Geology. doi:10.1130/G34387.1.

Livsey, Daniel, Alexander R. Simms, Alexandra Hangsterfer, Robert A. Nisbet, and Regina Dewitt. In Review. Drought Modulated by Solar Output for the last 3,000 years in Southwest United States. *In Review*.

Mannino, Antonio and Paul A. Montagna. 1996. Fine-scale spatial variation of sediment composition and salinity in Nueces Bay of South Texas. Texas Journal of Science. v. 48. p. 35-47

Mayewski, Paul A., Eelco E. Rohling, J. Curt Stager, Wibjfrn Karle´n, Kirk A. Maasch, L. David Meeker, Eric A. Meyerson, Francoise Gasse, Shirley van Kreveld, Karin Holmgren, Julia Lee-Thorp, Gunhild Rosqvist, Frank Rack, Michael Staubwasser, Ralph R. Schneider, Eric J. Steig. 2004. Holocene Climate Variability. Quaternary Research. v. 62, p. 243-255.

Milligan, M.R and D.R. Lemons. 1998. A sequence stratigraphic overview of sandy and gravelly lacustrine deltas deposited along the eastern margin of late Pleistocene Lake Bonneville, Northern Utah and Southern Idaho. Modern and Ancient Lake Systems: New Problems and Perspectives. p. 105-129

Milliken, K.T., Anderson, J.B., Rodriguez, A.B., 2008. Record of dramatic Holocene environmental changes linked to eustasy and climate change in Calcasieu Lake, Louisiana. In: Anderson, J.B., Rodriguez, A.B. (Eds.), Response of Upper Gulf Coast Estuaries to Holocene Climate Change and Sea Level Rise. Geological Society of America Special Papers 443, Boulder, Colorado, pp. 43–64.

Nichols, Maynard M. 1989. Sediment Accumulation Rates and Relative Sea-level rise in Lagoons. Marine Geology. v. 88, p. 201-219.

Noren, Anders J., Paul R. Blerman, Eric J Steig, Andrea Lini, John Southon. 2002. Millennial-scale storminess variability in the northeastern United States during the Holocene Epoch. Nature. v. 419, p. 821-824.

O'Brien, S.R., P.A. Mayewski, L.D. Meeker, D.A. Meese, M.S. Twickler, S.I. Whitlow. 1995. Complexity of Holocene Climate as Reconstructed from a Greenland Ice Core. Science. v. 270. p. 1962-1964

Olariu, Cornel and Janok P. Bhattarcharya. 2006. Terminal Distributary Channels and Delta Front Architecture of River-Dominated Delta Systems. Journal of Sedimentary Research. v. 76, p. 212-223. doi: 10.21 10/jsr.2006.026

Pethick, John. 2001. Coastal management and sea-level rise. Catena. v. 42, p. 307-322.

Poore, R.Z., H.J. Dowsett, S. Verardo. 2003. Millenial- to century-scale variability in Gulf of Mexico Holocene climate records. Paleoceanography. v. 18. no. 2, 1048

Reimer, Paula J. ; Bard, Edouard ; Bayliss, Alex ; Beck, J. Warren ; Blackwell, Paul G. ; Bronk Ramsey, Christopher ; Buck, Caitlin E. ; Cheng, Hai ; Edwards, R. Lawrence ; Friedrich, Michael ; Grootes, Pieter M. ; Guilderson, Thomas P. ; Haflidason, Haflidi ; Hajdas, Irka ;Hatté, Christine ; Heaton, Timothy J. ; Hoffmann, Dirk L. ; Hogg, Alan G. ; Hughen, Konrad A.; Kaiser, K. Felix ; Kromer, Bernd ; Manning, Sturt W. ; Niu, Mu ; Reimer, Ron W. ; Richards, David A. ; Scott, E. Marian ; Southon, John R. ; Staff, Richard A. ; Turney, Christian S. M. ;van der Plicht, Johannes. 2013. IntCal13 and Marine13 radiocarbon age calibration curves, 0-50,000 years cal BP, Radiocarbon, 55 (4), pp. 1869-1887

Rodriguez, Antonio B., Michael D. Hamilton, John B. Anderson. 2000. Facies and evolution of the Modern Brazos Delta, Texas: Wave Versus Flood Influence. Journal of Sedimentary Research. v. 70, no. 2, p. 283-295

Rodriguez, A.B., Greene, D.L.J., Anderson, J.B., Simms, A.R., 2008. Response of Mobile Bay and eastern Mississippi Sound, Alabama, to changes in sediment accommodation and accumulation. In: Anderson, J.B., Rodriguez, A.B. (Eds.), Response of Upper Gulf Coast Estuaries to Holocene Climate Change and Sea Level Rise. Geological Society of America Special Papers 443, Boulder, Colorado, pp. 13–30.

Rodriguez, Antonio B., Alexander R. Simms, John B. Anderson. 2010. Bayhead deltas across the northern Gulf of Mexico back step in response to the 8.2 ka cooling event. Quaternary Science Reviews. v. 29, i. 27-28, p. 3983-3993.

Shideler, G.L., 1984. Suspended sediment responses in a wind-dominated estuary of the Texas Gulf Coast. Journal of Sedimentary Petrology. v. 54 p. 731-745

Shen, Zhixiong, Torbjörn Törnqvist, Barbara Mauz. 2015. Episodic overbank deposition as a dominant mechanism of floodplain and delta-plain aggradation. Geology. v. 43 no. 10 p. 875-878

Simms, Alexander R., John B. Anderson, Michael Blum. 2006. Barrier-island aggradation via inlet migration: Mustang Island, Texas. Sedimentary Geology. v. 187, p. 105-126

Simms, Alexander R., Kurt Lambeck, Anthony Purcell, John B. Anderson, Antonio B. Rodriguez. 2007. Sea-level history of the Gulf of Mexico since the Last Glacial Maximum with implications for the melting history of the Laurentide Ice Sheet. Quaternary Science Reviews. v. 26, p. 920-940.

Simms, Alexander R., John B. Anderson, Antonio B. Rodriguez, Marco Taviani. 2008. Mechanisms controlling environmental change within an estuary: Corpus Christi Bay, Texas, USA. The Geological Society of America: Special Paper 443.

Simms, Alexander R., Niranjan Aryal, Yusuke Yokoyama, Hiroyuki Matsuzaki, and Regina DeWitt. 2009. Insights on a Proposed Mid-Holocene Highstand along the Northwestern Gulf of Mexico from the Evolution of Small Coastal Ponds. Journal of Sedimentary Research. v. 79, p. 757-772. doi: 10.2110/jsr.2009.079

Simms, Alexander R., Niranjan Aryal, Lauren Miller, and Yusuke Yokoyama. 2010. The incised valley of Baffin Bay, Texas: a tale of two climates. Sedimentology. v. 57, p. 642-669. doi: 10.1111/j.1365-3091.2009.01111.x

Stuiver, M., Reimer, P.J., Bard, E., Beck, J.W., Burr, G.S., Hughen, K.A., Kromer, B., McCormac, G., van der Plicht, J., Spurk, M., 1998. INTCAL98 radiocarbon age calibration, 24,000-0 cal BP. Radiocarbon 40, 1041–1083.

Texas Commission on Environmental Quality (TCEQ). 2013. http://www.tceq.texas.gov/assets /public/ compliance/monops/water/02twqmar/basin21.pdf. Viewed on 4/1/2014.

Törnqvist, Torbjörn E., Juan L. González, Lee A. Newsom, Klaas van der Borg, Arie F.M. de Jong and Charles W. Kurnik. 20o4. Deciphering Holocene sea-level history on the U.S. Gulf Coast: A high-resolution record from the Mississippi Delta. Geological Society of America Bulletin. v. 116, p. 1026-1039.

Toomey, R.S. III, Michael D. Blum, Salvatore Valestro Jr. 1993. Late Quaternary climates and environments of the Edwards Plateau, Texas. Global and Planetary Change. v. 7, i. 4, p. 299-320.

Troiani, B.T., A.R. Simms, T. Dellapenna, E. Piper, Y. Yokoyama. 2011. The importance of sea-level and climate change, including changing wind energy, on the evolution of a coastal estuary: Copano Bay, Texas. Marine Geology. v. 280.1 p. 1-19

United States Geological Survey (USGS). Viewed on 4/10/2014. http://pubs.usgs.gov/fs/fs-081-01/fs_081-01.htm

Mitchum, Jr., R.M., P.R.Vail, J.B. Sangree. 1977. Seismic Stratigraphy and Global Changes of Sea Level, Part 6: Stratigraphic Interpretation of Seismic Reflection Patterns in Depositional Sequences. Seismic Stratigraphy – Applications to Hydrocarbon Exploration. AAPG Memoir 26. p. 117-133

Van Heerden, Ivor Ll., Harry H. Roberts. 1988. Facies Develoopment of Atchafalaya Delta, Louisiana: A Modern Bayhead Delta. AAPG Bulletin. v. 72 no. 4 p.439-453

Wallace, Davin J., John B. Anderson, Antonio B. Rodriguez. 2009. Natural versus anthropogenic mechanisms of erosion along the upper Texas coast. The Geological Society of America. Special Paper 460. p. 137-147

White, William A., Robert A. Morton, Charles W. Holmes. 2002. A comparison of factors controlling sedimentation rates and wetland loss in fluvial-deltaic, Texas Gulf coast. Geomorphology. v. 44, p. 47-66

Yang, S.L., I.M. Belkin, A.I. Belkina, Q.Y. Zhao, J. Zhu, P.X. Ding. 2003. Delta response to decline in sediment supply from the Yangtze River: Evidence of the recent four decades and expectations for the next half-century. Estuarine Coastal and Shelf Science. v.57. p. 689-699

Figures

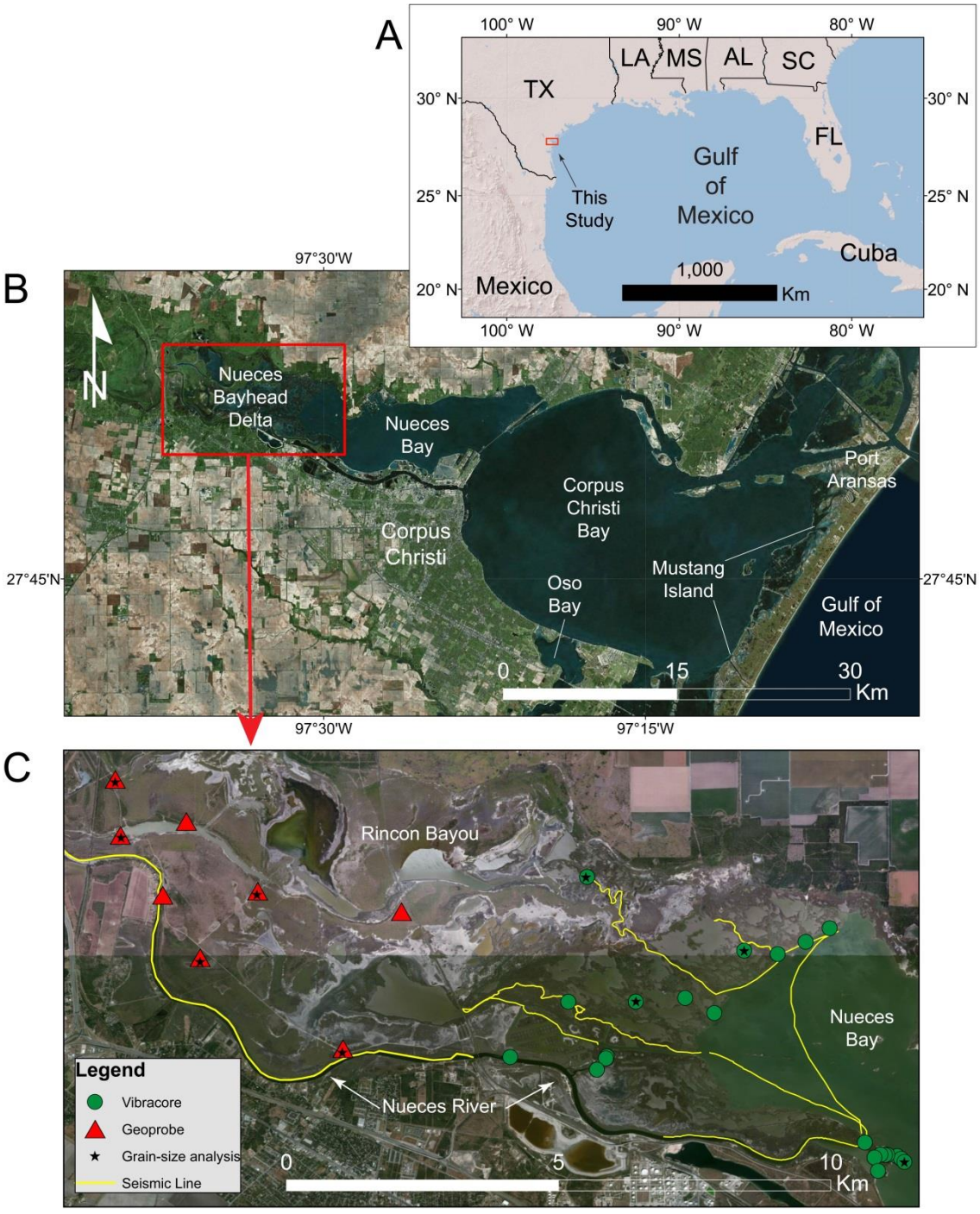

Figure 1. A) General location of the study area within the Gulf of Mexico **B)** Satellite imagery of the study area including the Nueces Bayhead delta, Corpus Christi Bay (central basin), and Mustang Island (barrier island). **C)** Locations of the cores, cores used for grain-size analysis, and seismic data for this study.

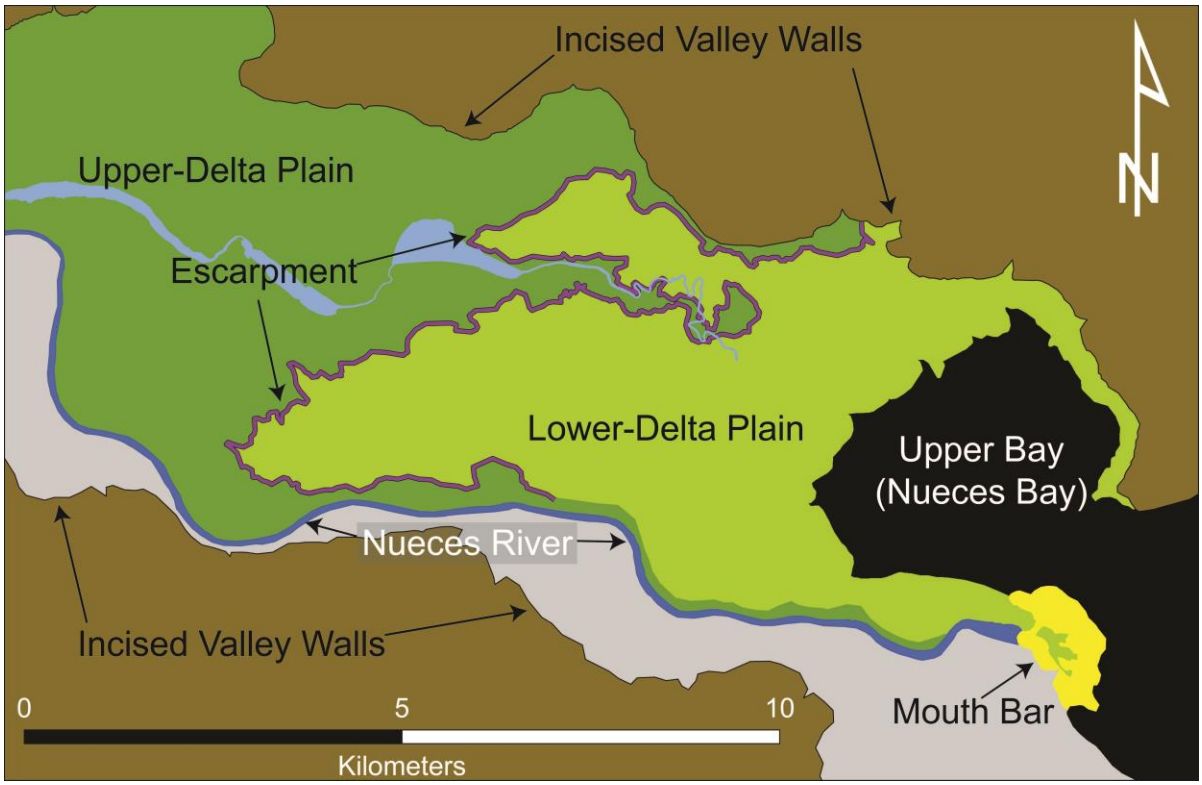

Figure 2. Modern distribution of the five major depositional environments defined based on the characterization of nine sedimentary facies and five seismic facies. A notable scarp (purple line) separates the lower-delta plain from the upper-delta plain. The grey area represents an area of high anthropogenic modidification.

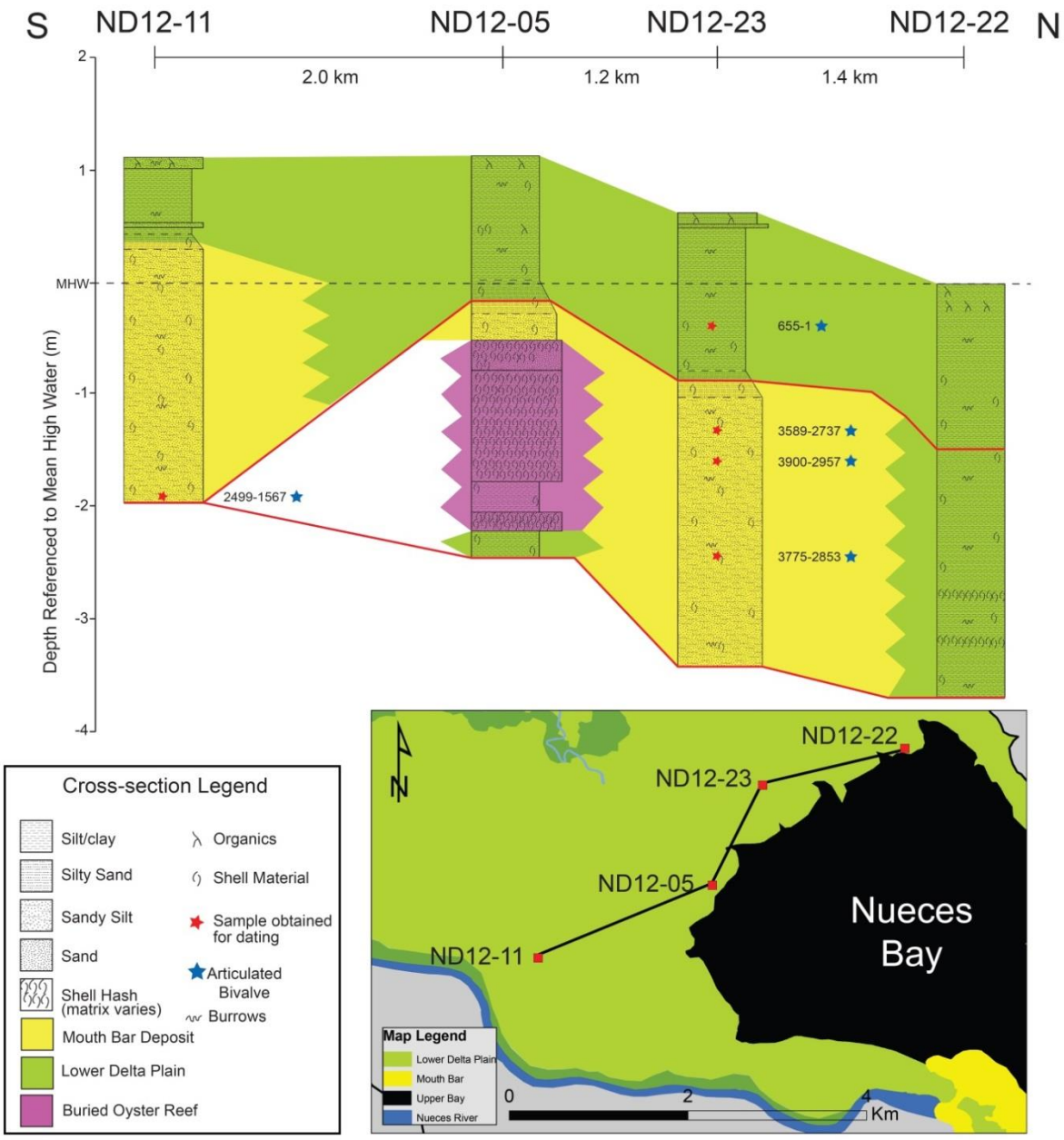

Figure 3. Strike oriented cross-section of the Nueces Bayhead Delta.

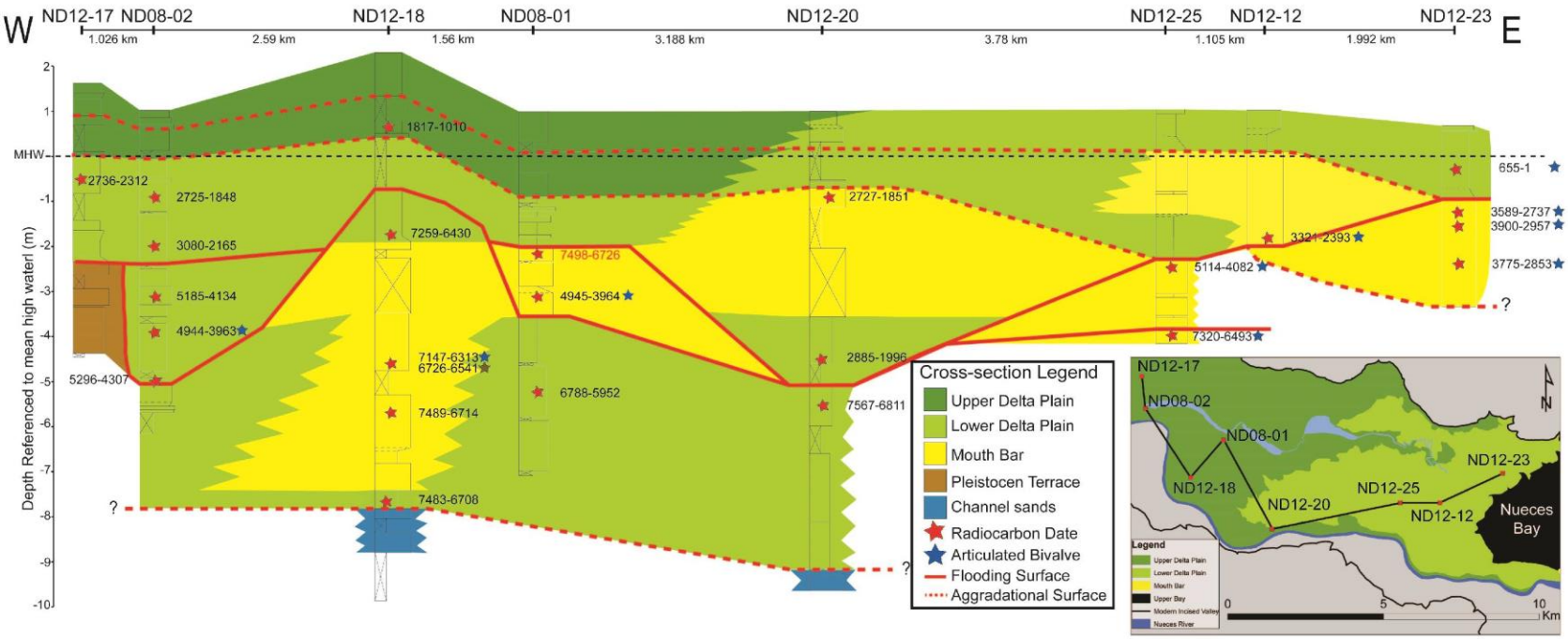

Figure 4. Dip-oriented profile through the Nueces Bayhead Delta. Red stars indicate the location of radiocarbon ages. The upper-most age (in red) in core ND08-01 was not used for the deltaic evolution interpretation due to the age not being in stratigraphic order relative to the other ages in the core.

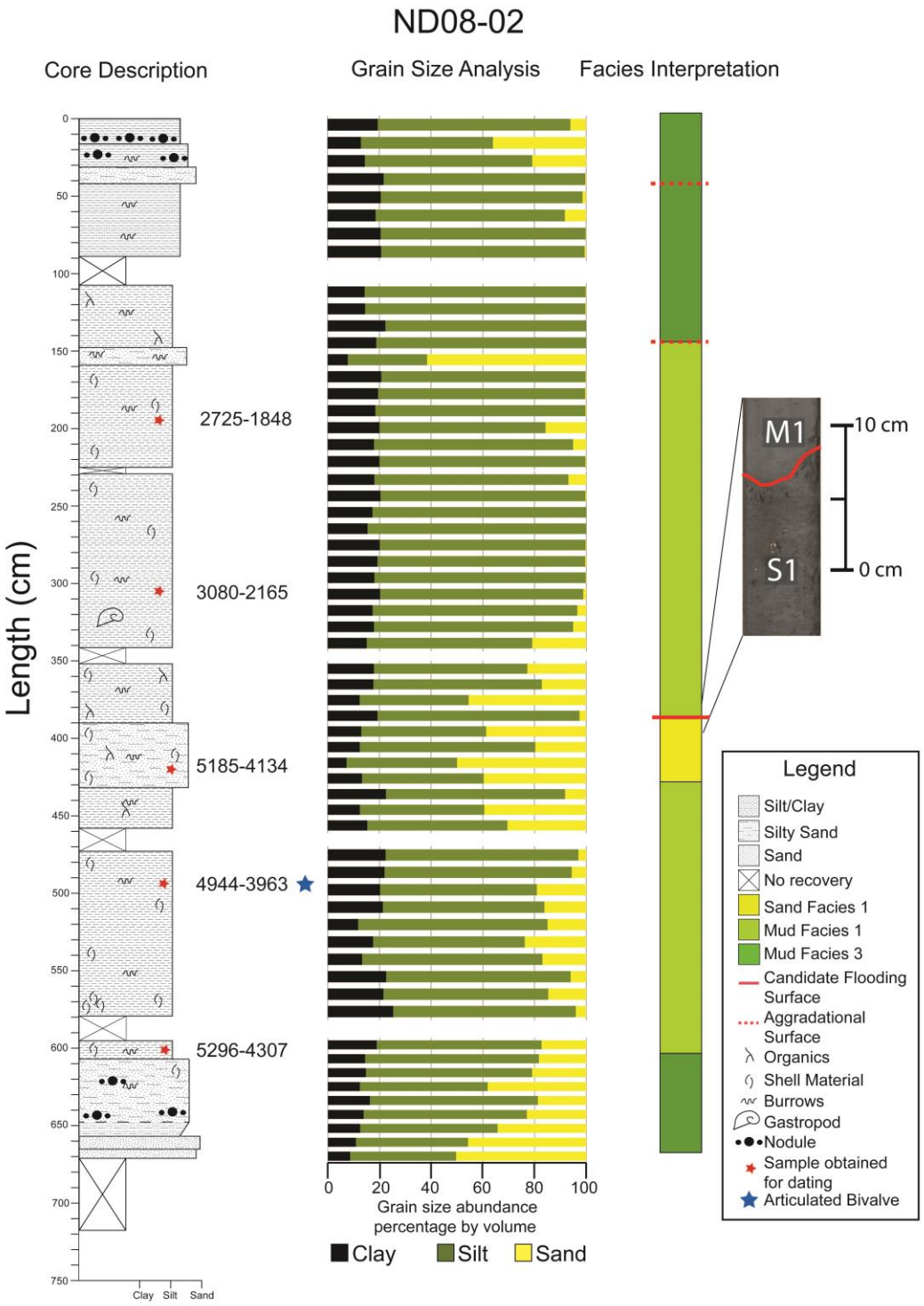

Figure 5. Core description (left), grain-size profile (right), and facies interpretation (right) of core ND08-02. Locations of radiocarbon dates are noted with red stars. See Appendix B for core location.

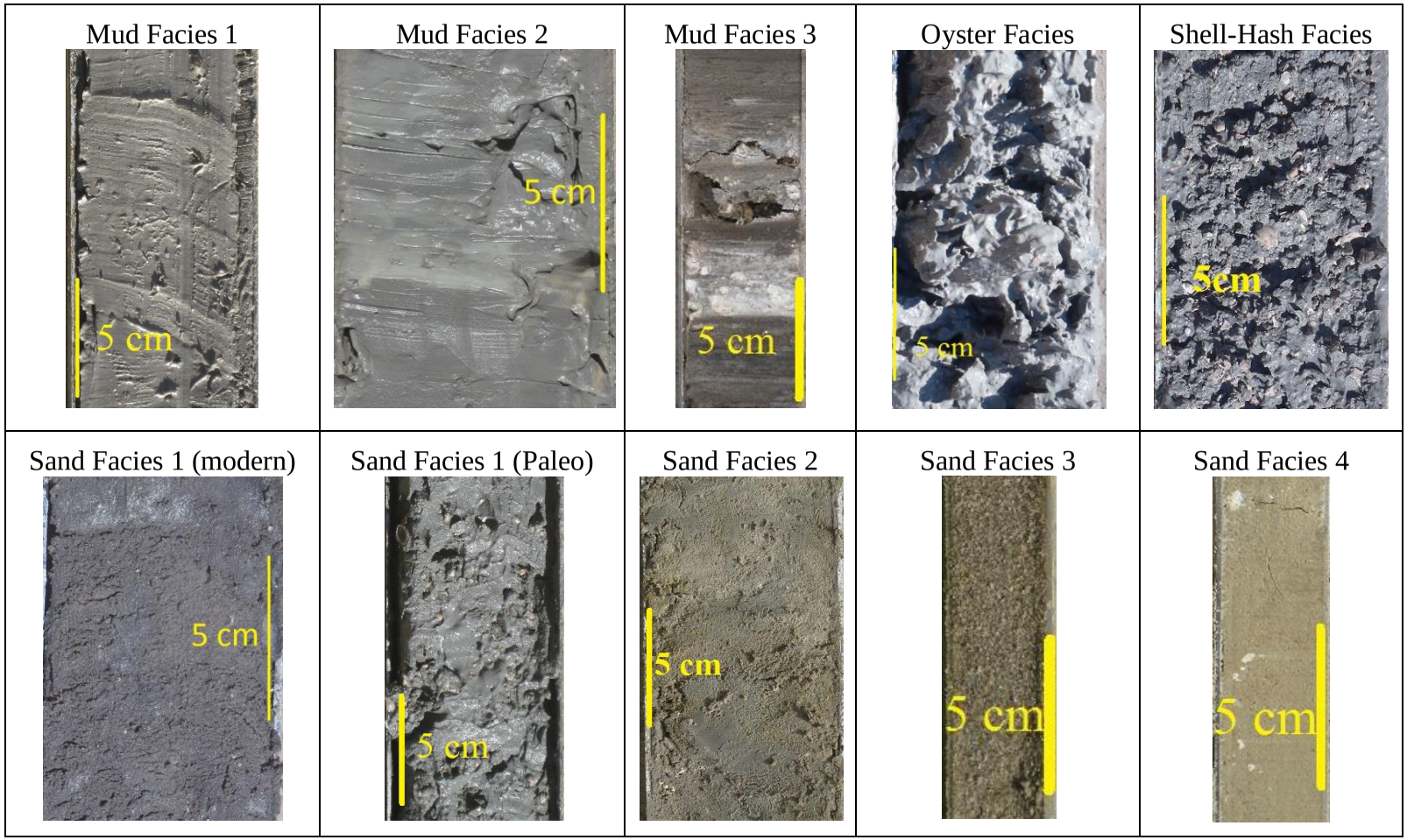

Figure 6. Photographs of facies identified in this study.

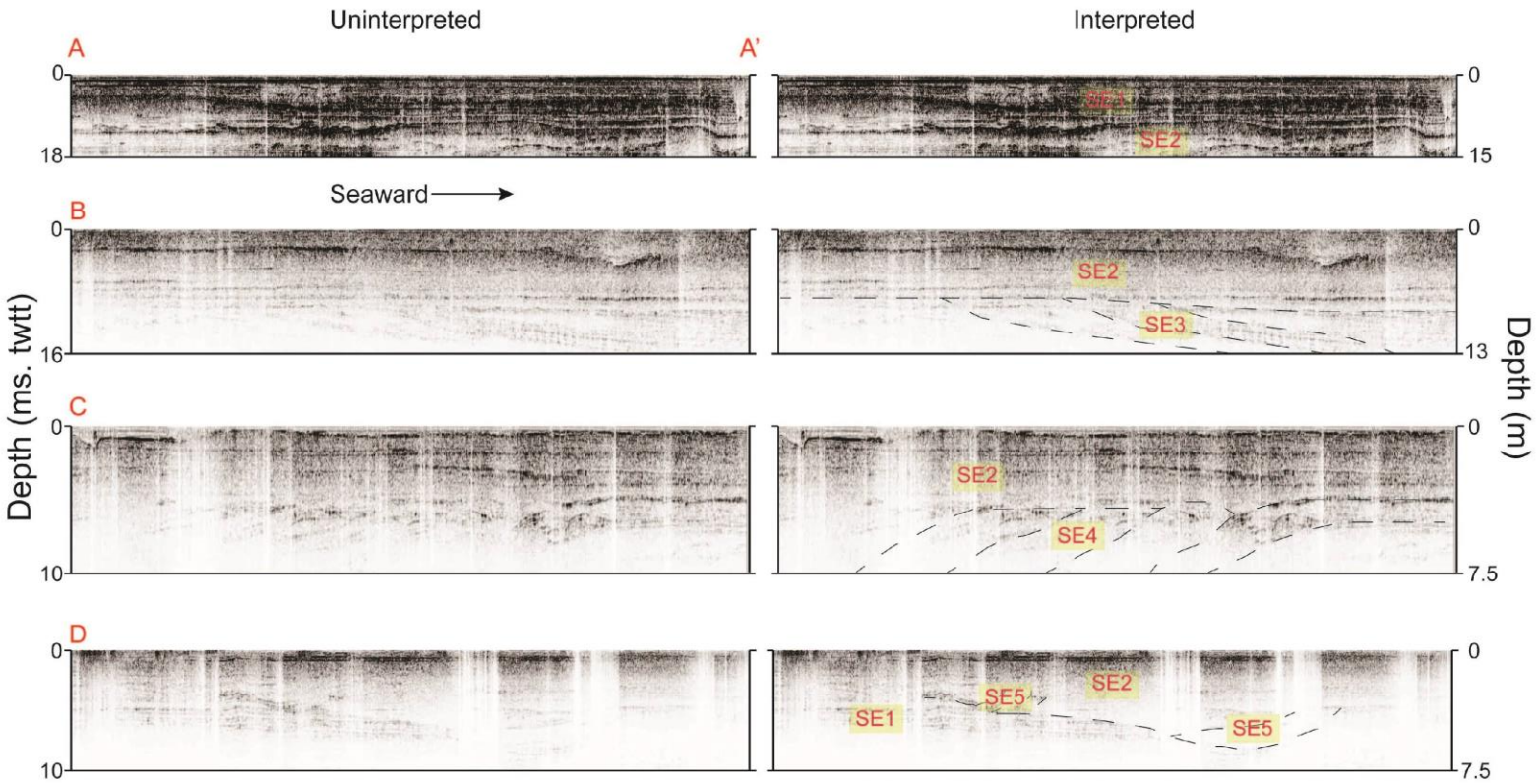

Figure 7. Un-interpreted (left) and interpreted (right) seismic profiles illustrating the seismic facies identified in this study.

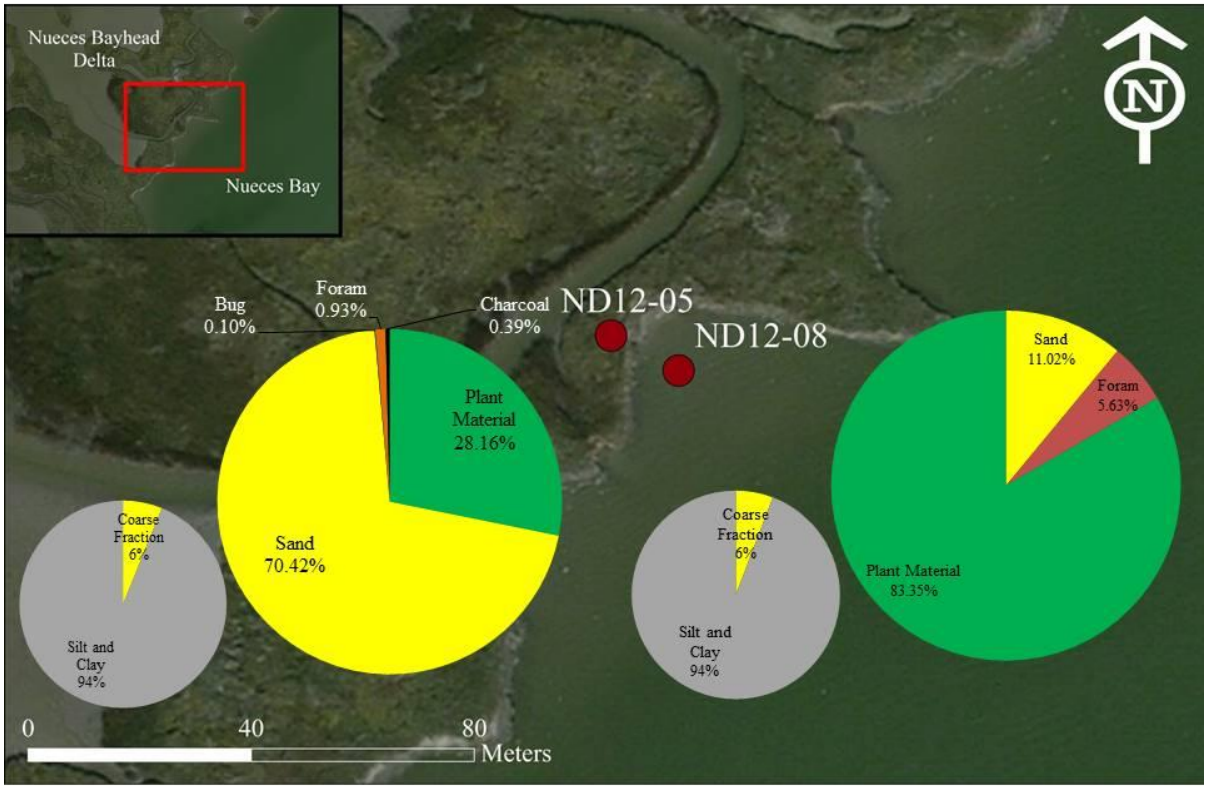

Figure 8. Coarse fraction analysis results from two core tops within the lower delta plain (ND12-05) and the upper bay (ND12-08). Both cores were sampled at a depth of 5cm and both cores have similar grain size.

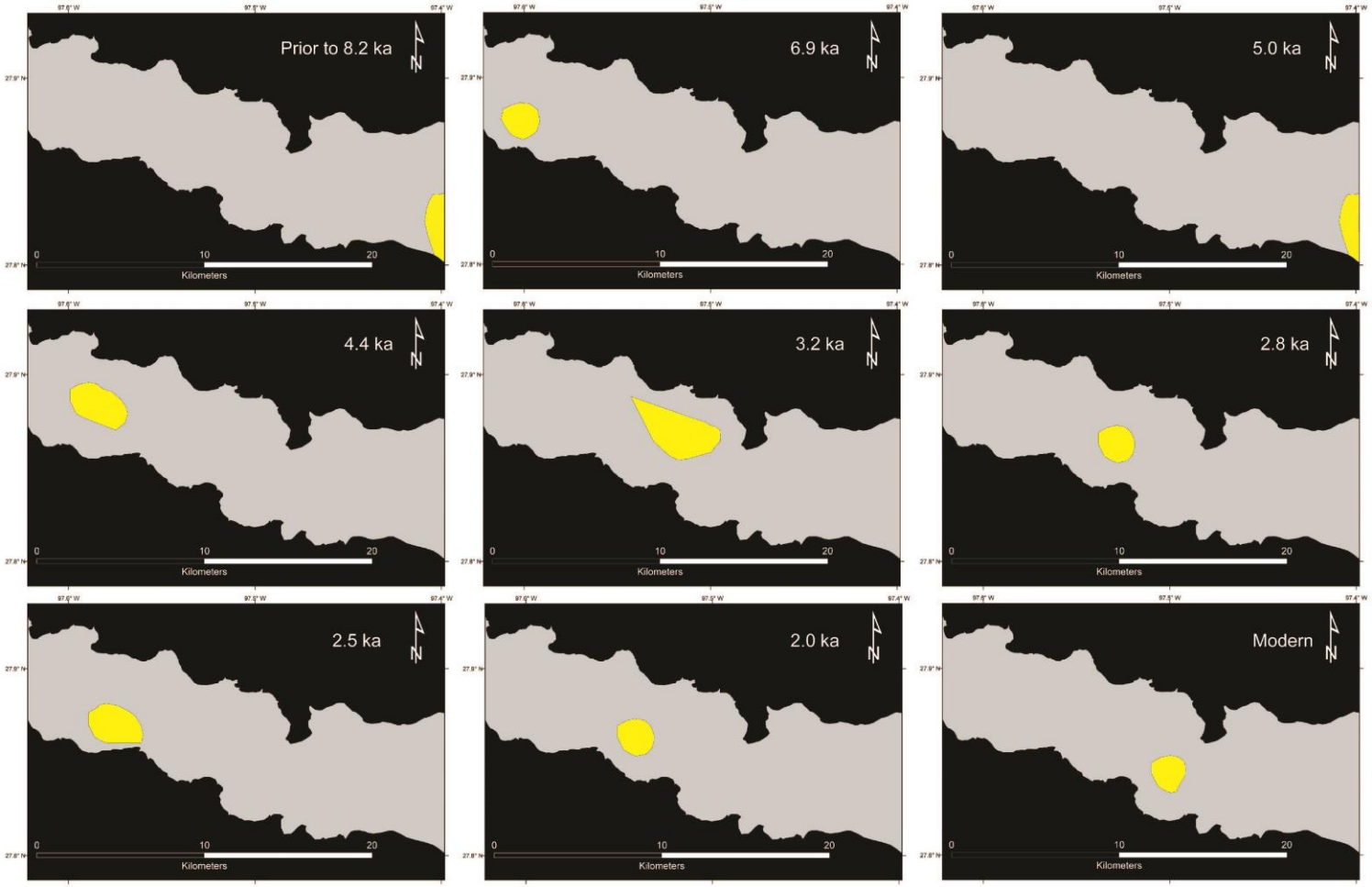

Figure 9. Paleo-geographic maps showing the locations of the Nueces Bayhead Delta mouth bars over the last 8 ka.

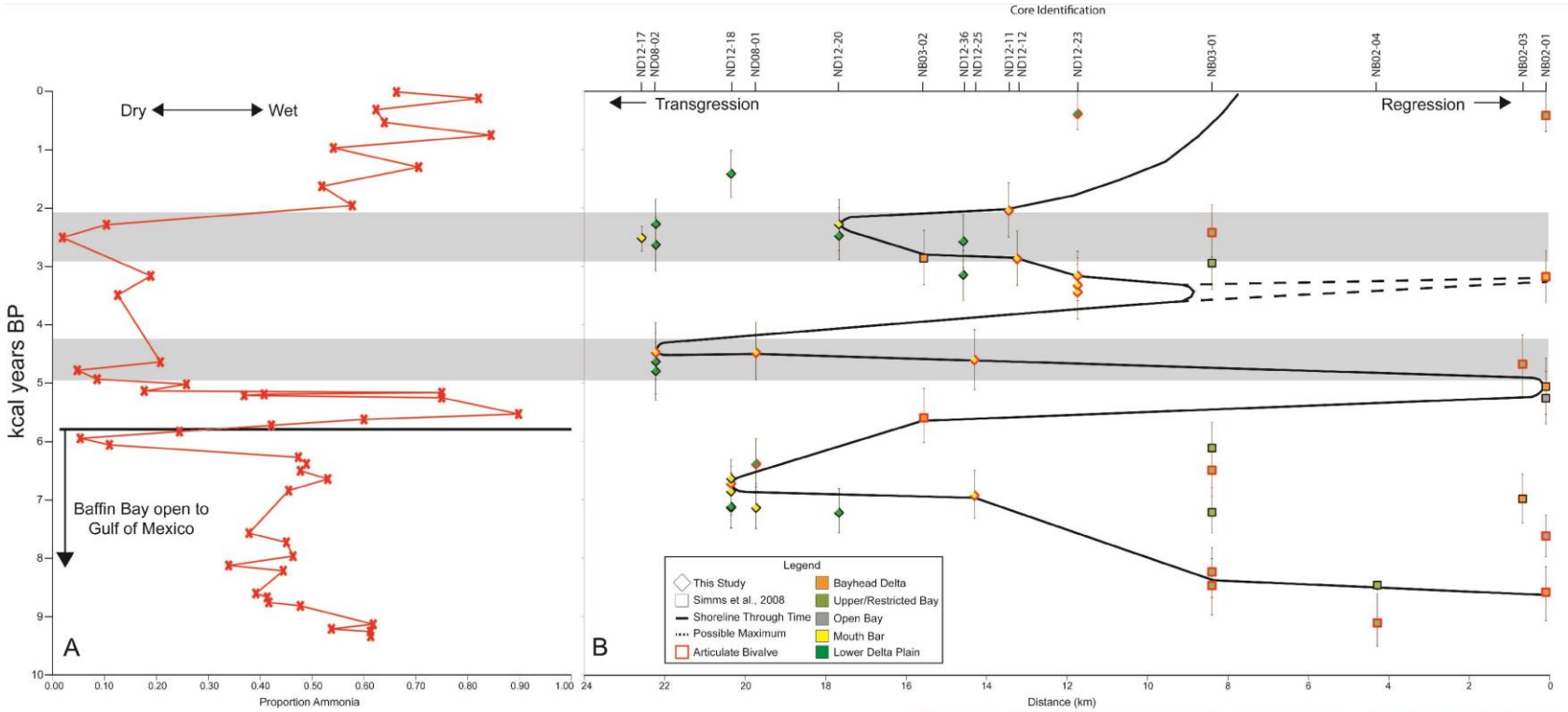

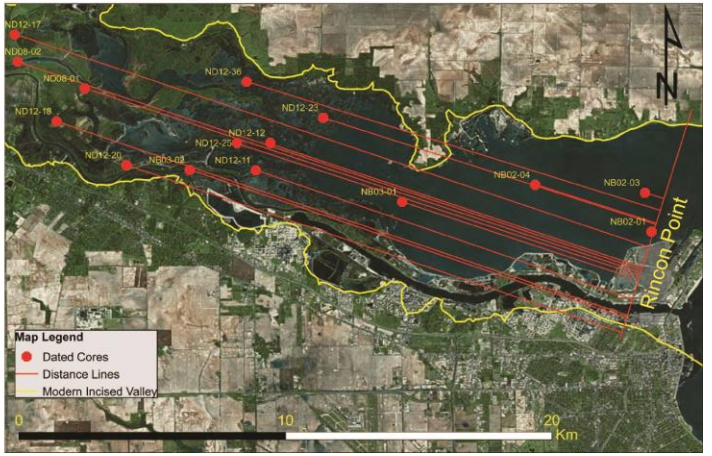

Figure 10. A) The proportion of *Ammonia sp.* foraminifera species used as a proxy for periods of aridity and more mesic conditions (Buzas-Stephens et al., 2014). **B)** The shoreline position of the bayhead delta through time. The error bars illustrate the two-sigma distribution of the radiocarbon age. **C)** Arial imagery of the Nueces Bayhead Delta and upper Nueces Bay indicating the position of the sediment cores. Note the position of **Rincon Point** for the deltaic evolution chapter.

Lab Code	Core	Depth (cm)	Depth Relative to MHW (cm)	Articulated	Species	^{14}C Age	^{14}C Error	Marine Reservoir	Reservoir Error	Age Distribution (Cal yrs BP)	Median Probability (Cal yrs BP)
D-AMS 009133	ND08-01	317.3	-213.3	no	*Rangia flexuosa*	6566	25	365	182.5	7498 - 6726	7139
D-AMS 009134	ND08-01	413.2	-309.2	yes	*Macoma tageliformis*	4268	20	365	182.5	4945 - 3964	4478
D-AMS 011360	ND08-01	498.1	-394.1	yes	*Rangia flexuosa*	5884	28	365	182.5	6788 - 5952	6386
D-AMS 009135	ND08-02	193.68	-84.68	no	*Macoma tageliformis*	2514	20	365	182.5	2725 - 1848	2274
D-AMS 009136	ND08-02	305.58	-196.58	no	*Macoma tageliformis*	2815	19	365	182.5	3080 - 2165	2629
D-AMS 009138	ND08-02	419.48	-310.48	no	*Rangia flexuosa*	4388	22	365	182.5	5185 - 4134	4633
D-AMS 009137	ND08-02	494.38	-385.38	yes	*Macoma tageliformis*	4267	22	365	182.5	4944 - 3963	4477
D-AMS 009139	ND08-02	601.28	-492.28	no	*Rangia flexuosa*	4510	38	365	182.5	5296 - 4307	4796
YAUT-007632	ND12-17	153	8	N/A	gastropod‡	2561	19	365	182.5	2736 - 2312	2511
D-AMS 009141	ND12-18	157.4	-155.08	N/A	pincer	1768	22	365	182.5	1817 - 1010	1410
D-AMS 011361	ND12-18	408.8	-406.48	N/A	forams	6304	32	365	182.5	7259 - 6430	6857
D-AMS 009142	ND12-18	703.1	-700.78	yes	*Macoma tageliformis*	6186	28	365	182.5	7147 - 6313	6722
D-AMS 009145	ND12-18	703.1	-700.78	N/A	wood	5821	28	0	0	6726 - 6541	6637
D-AMS 009143	ND12-18	796.98	-794.66	no	*Macoma tageliformis*	6555	27	365	182.5	7489 - 6714	7127
D-AMS 009144	ND12-18	1012.38	-1010.06	no	*Rangia flexuosa*	6549	25	365	182.5	7483 - 6708	7121

Lab Code	Core	Depth (cm)	Depth Relative to MHW (cm)	Articulated	Species	^{14}C Age	^{14}C Error	Marine Reservoir	Reservoir Error	Age Distribution (Cal yrs BP)	Median Probability (Cal yrs BP)
D-AMS 009140	ND12-20	219.4	-113.4	no	*Rangia flexuosa*	2518	22	365	182.5	2727 - 1851	2279
YAUT-007633	ND12-20	502.2	-396.2	no	*Rangia flexuosa*	2675	20	365	182.5	2885 - 1996	2473
YAUT-007634	ND12-20	647.2	-541.2	no	*Macoma tenta*	6644	24	365	182.5	7567 - 6811	7222
D-AMS 011362	ND12-11	274	-164	yes	*Mulinia lateralis*	2326	25	365	182.5	2499 - 1567	2043
D-AMS 011359	ND12-12	287	-171	yes	*Mulinia lateralis*	2997	26	365	182.5	3321 - 2393	2869
YAUT-007635	ND12-23	100	-22	yes	*Macoma tenta*	697	18	365	182.5	655 - 1	384
YAUT-007636	ND12-23	191	-113	yes	*Rangia flexuosa*	3249	21	365	182.5	3589 - 2737	3161
YAUT-007637	ND12-23	222	-144	yes	*Rangia flexuosa*	3475	23	365	182.5	3900 - 2957	3442
YAUT-007638	ND12-23	301	-223	yes	*Rangia flexuosa*	3380	20	365	182.5	3775 - 2853	3320
D-AMS 011357	ND12-25	357	-252	yes	*Tagelus plebius*	4365	28	365	182.5	5114 - 4082	4604
D-AMS 011358	ND12-25	499	-394	yes	*Mulinia lateralis*	6368	30	365	182.5	7320 - 6493	6929
D-AMS 011355	ND12-36	49	39	no	*Mulinia lateralis*	3234	24	365	182.5	3576 - 2728	3144
D-AMS 011356	ND12-36	138	-50	no	*Mulinia lateralis*	2765	22	365	182.5	3024 - 2114	2570

Table 1.(pages 36 and 37) Radiocarbon ages for this study. Dates were calibrated using CALIB v7.0.2. Samples that begin with 'YAUT' were processed by Dr. Yusuke Yokoyama. The samples that begin with 'D-AMS' were processed by DirectAMS.
‡ = Unable to identify gastropod but assumed terrestrial given the location from which it came.

	Total Volume ($x10^8$ m^3)					Sand Volume (%)		
Time (ka)	Minimum ($U_u - U_l$)	Maximum ($V_u - V_l$)	Average (V_a)	Percent Mouth Bar (M)	Percent Lower-Delta Plain (LDP)	Mouth Bar (S_m)	Lower-Delta Plain (S_{lsp})	Sand Supply per Year ($x10^3$ m^3/yr)
4.8 - 3.2	1.30	1.76	1.53	18	82	50	3	11.0 +/- 2.4
3.2 - 2.6	0.72	1.00	0.86	4	96	50	3	5.9 +/- 2.4
2.6 - 0.0	0.99	1.33	1.16	18	82	50	3	5.3 +/- 1.1

Table 2.Values used for sediment supply calculations

Facies	Brief Description	Environment
Mud Facies 1	Grey clayey silt; maximum 5% shells by volume	Lower Delta Plain – Sub-aerial/intermittent marine/fluvial
Mud Facies 2	Laminated light and dark grey silty clay	Lower Delta Plain – tidal distributary
Mud Facies 3	Black/dark grey clayey silt; organics present	Upper Delta Plain
Sand Facies 1	Structureless silty sand to sand	Mouth Bar
Sand Facies 2	Mottled brown and grey silty sand	Lower Delta Plain – Levee
Sand Facies 3	Very fine to fine brown sand; no shell material	Fluvial – Channel
Sand Facies 4	Very fine tan sand, $CaCO_3$ nodules observed	Fluvial – Pleistocene terrace
Oyster Facies	Composed of articulated clusters of oysters	Oyster Reef – Proximal reef
Shell Hash Facies	>80% shell fragments by volume	Oyster Reef – Distal reef
Seismic Facies 1	High amplitude parallel reflections	Upper Bay
Seismic Facies 2	Chaotic to transparent reflections	Mouth Bar
Seismic Facies 3	Series of dipping, en echelon reflections	Lower-Delta Plain
Seismic Facies 4	Sets of complex sigmoid oblique reflections	Fluvial
Seismic Facies 5	Prograded fill reflections	Fluvial

Table 3. Table showing the facies this study defined and the environments they represent.

Appendix A

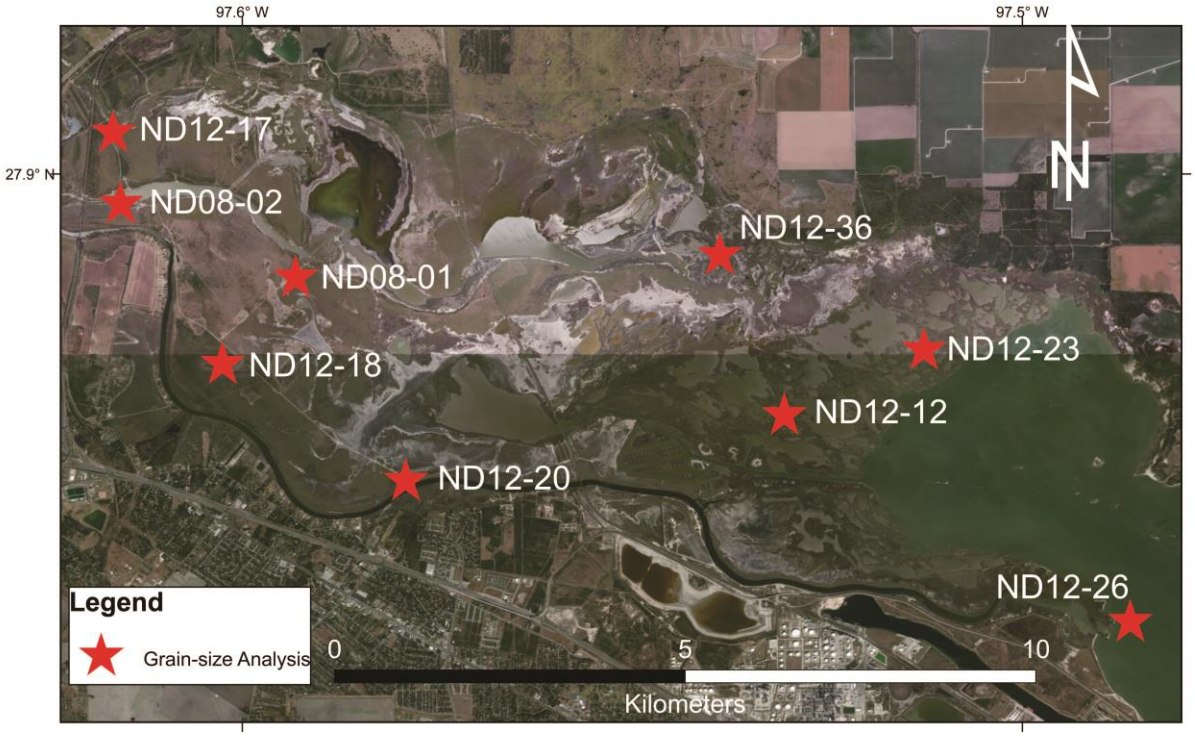

Grain-size analysis was performed on five geoprobe cores and four vibracores. The five geoprobe cores were sampled at 10 cm intervals and the vibracores were sampled at 25 cm intervals. The map illustrates the locations of cores that with grain-size analysis from the Nueces Bayhead Delta

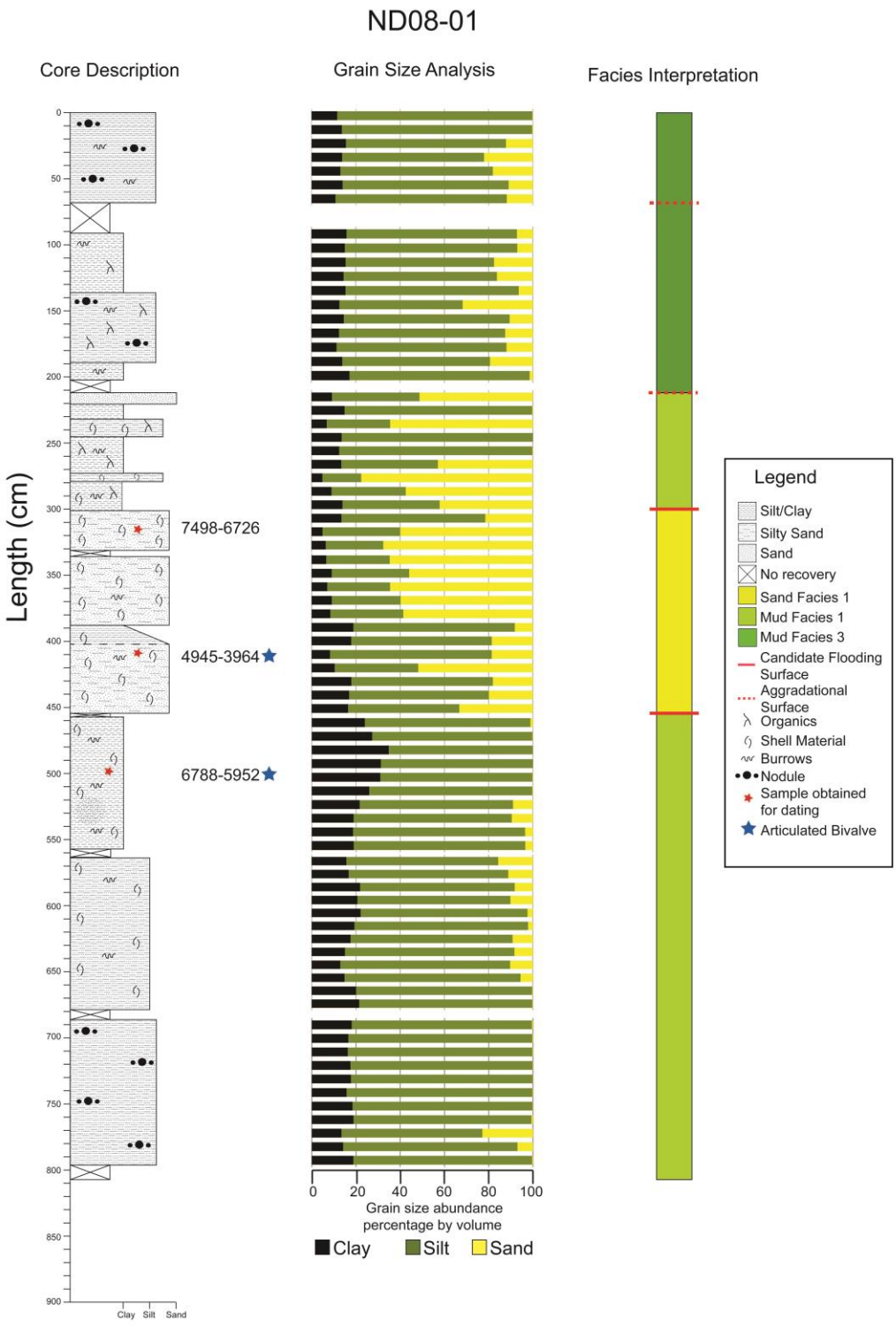

The **left image** shows the description of the core and where shells and organics were observed. The radiocarbon dates that were obtained from this core are noted with red stars. The **middle image** illustrates the grain-size distribution and the **right image** provides the facies.

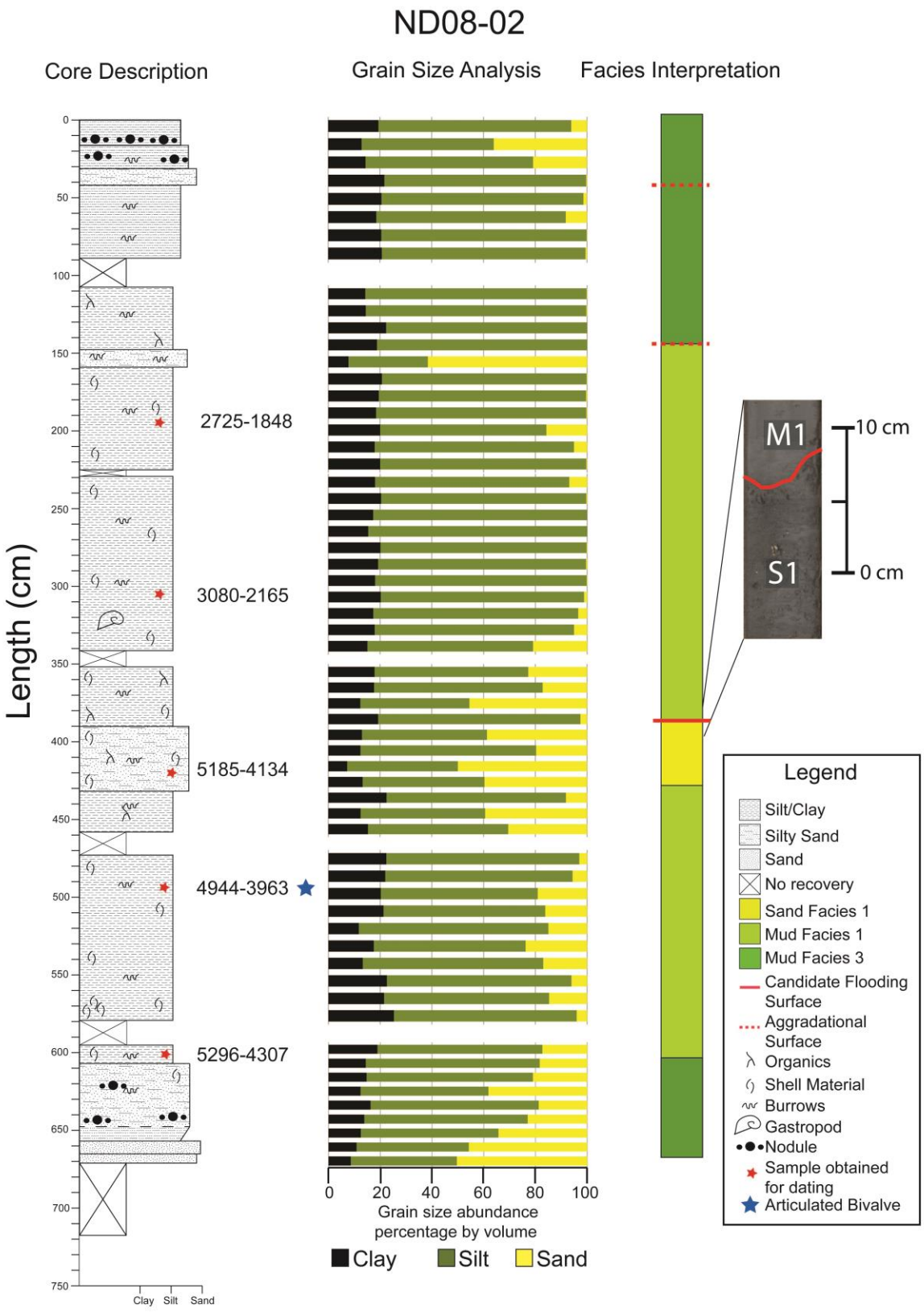

See page 38 for description.

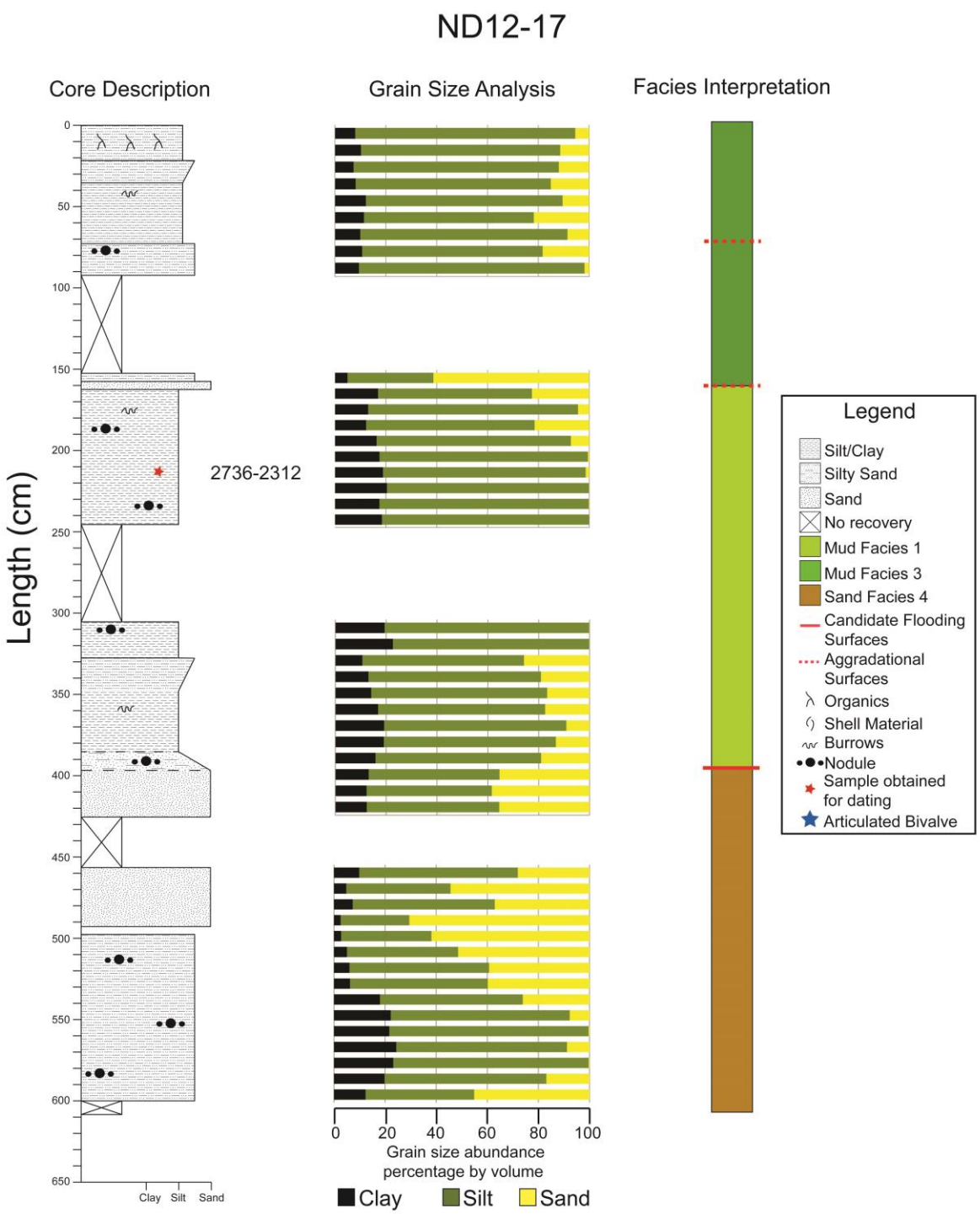

See page 38 for description.

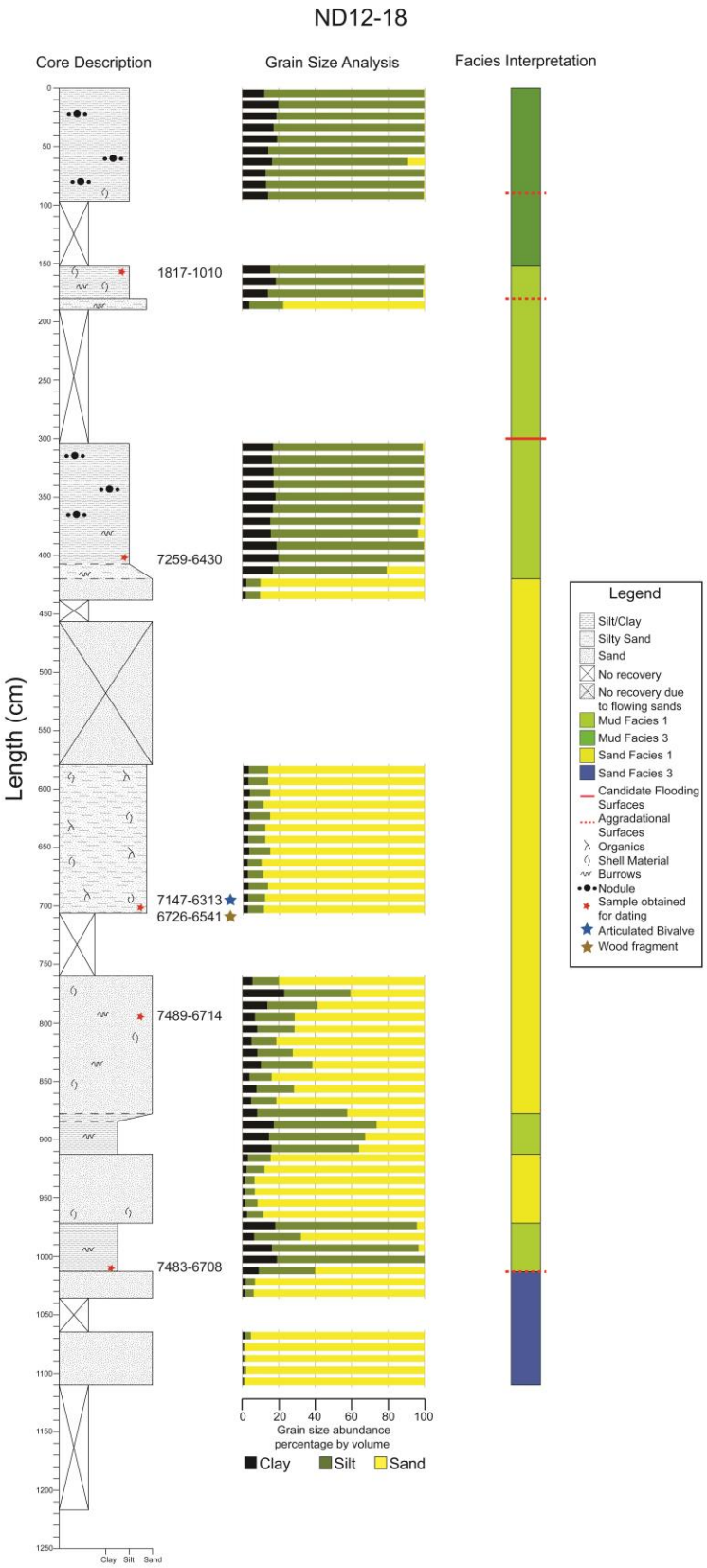

See page 38 for description.

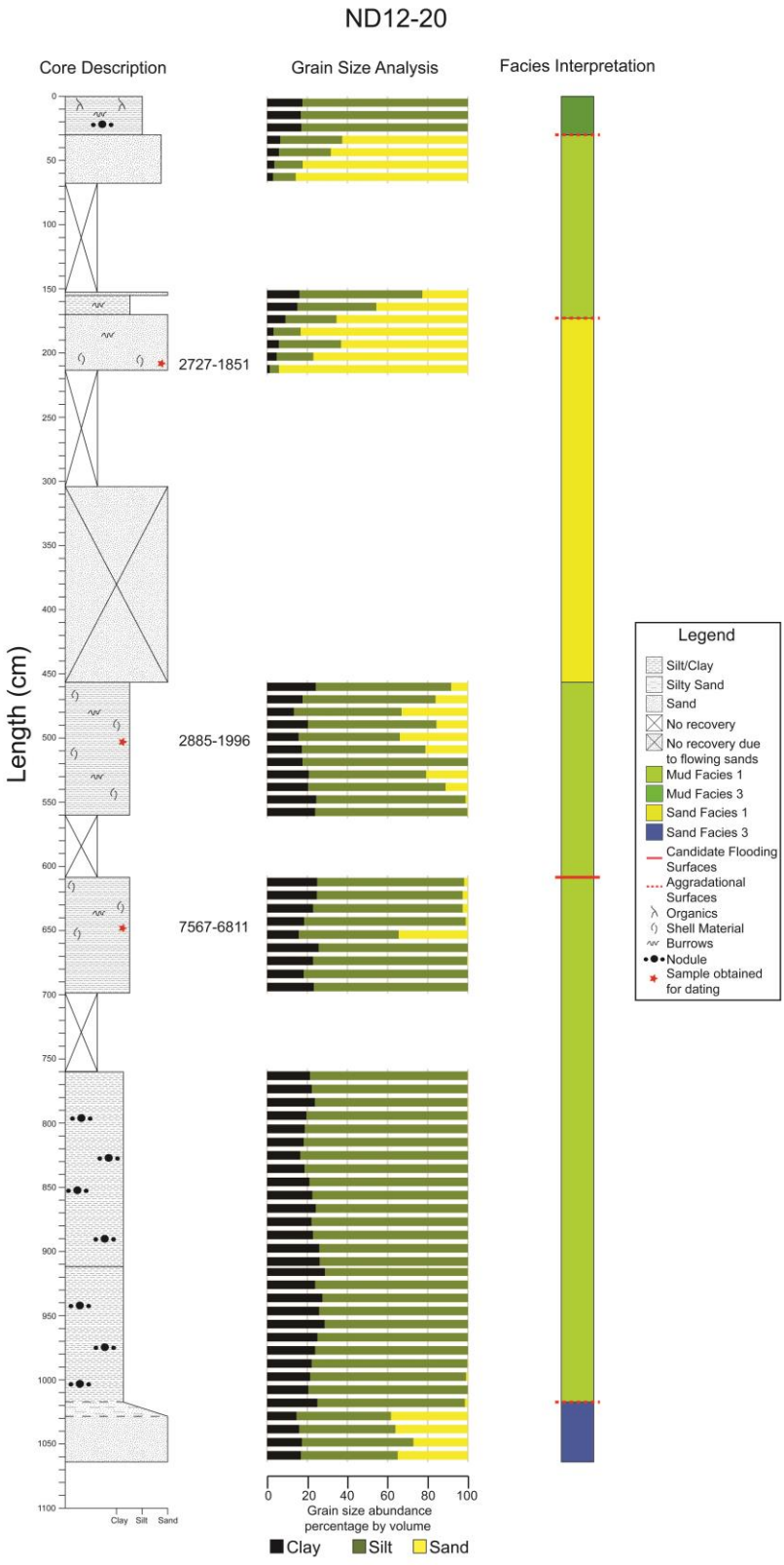

See page 38 for description.

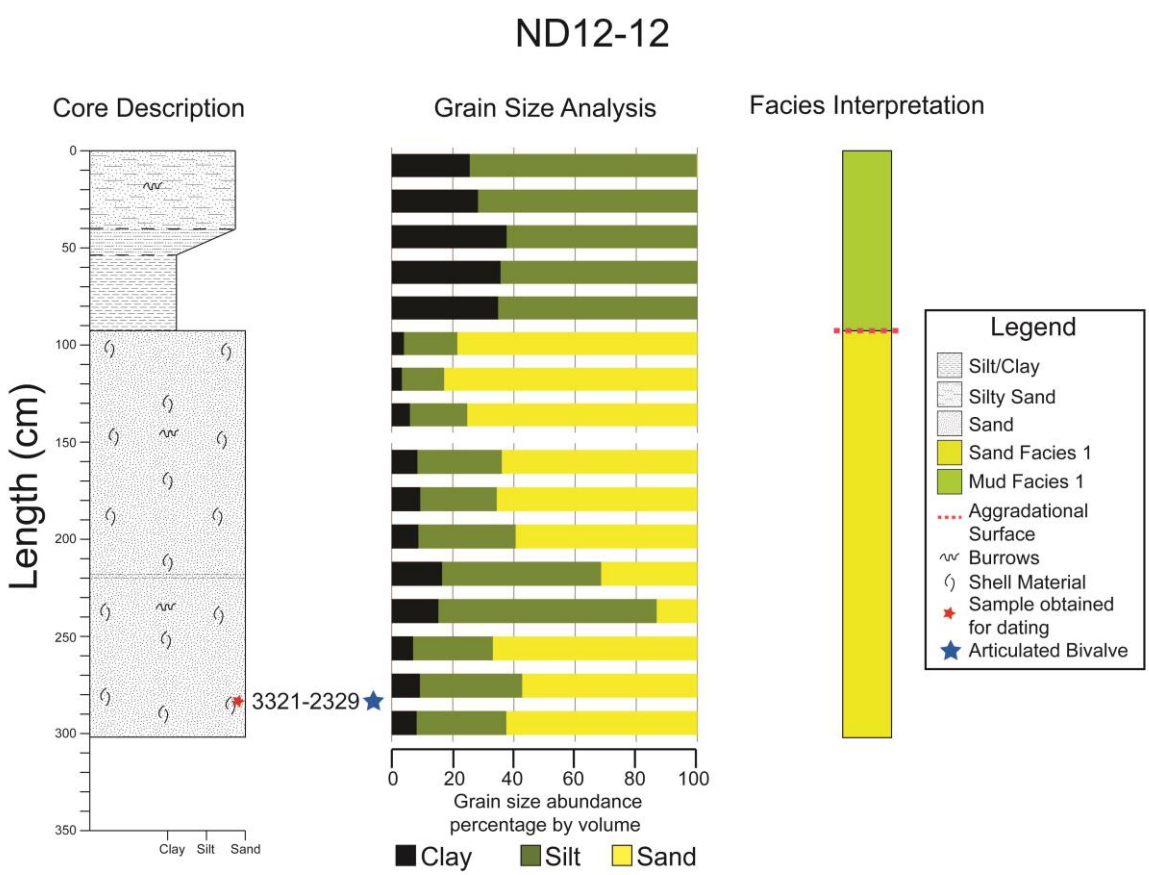

See page 38 for description.

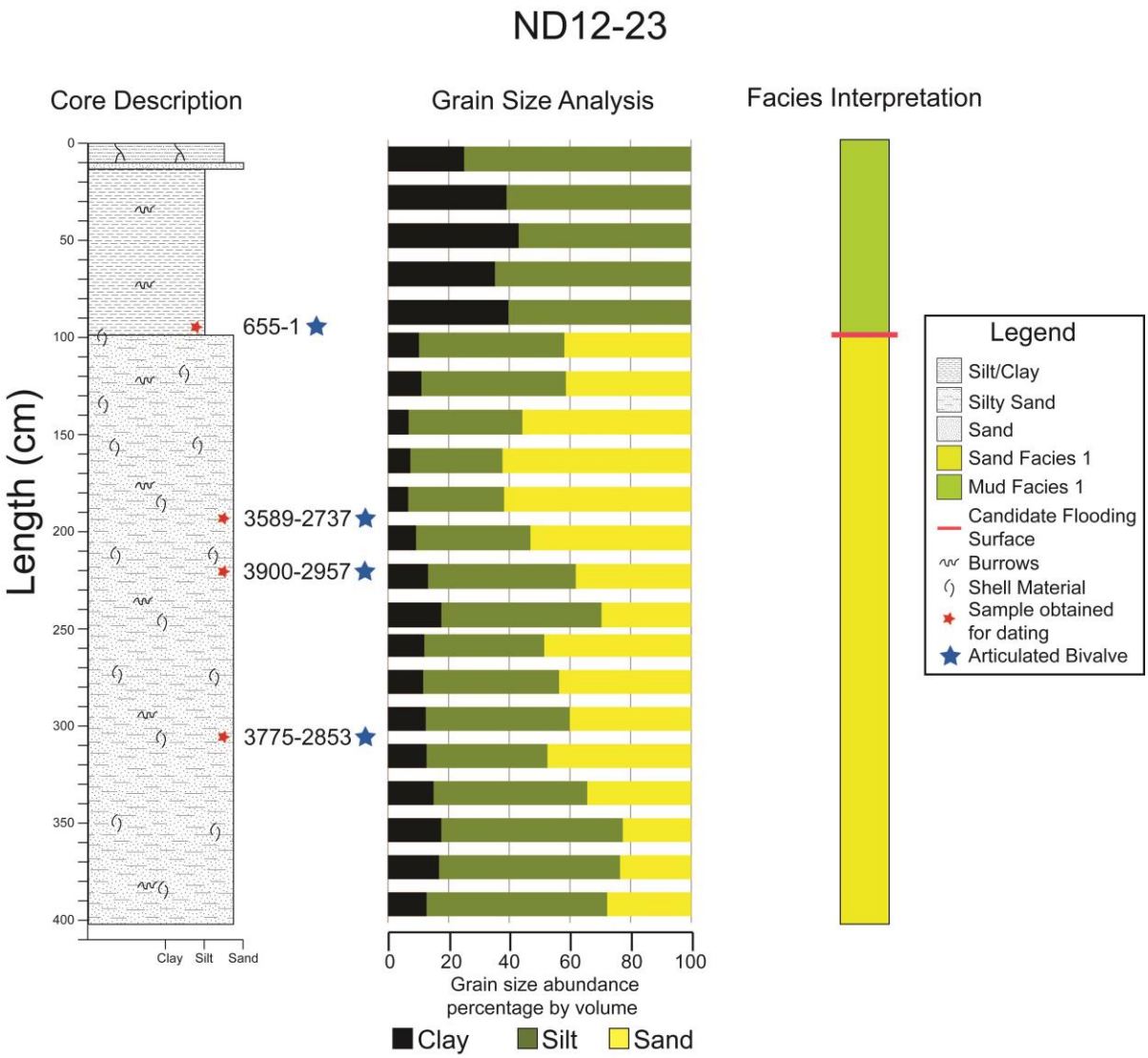

See page 38 for description.

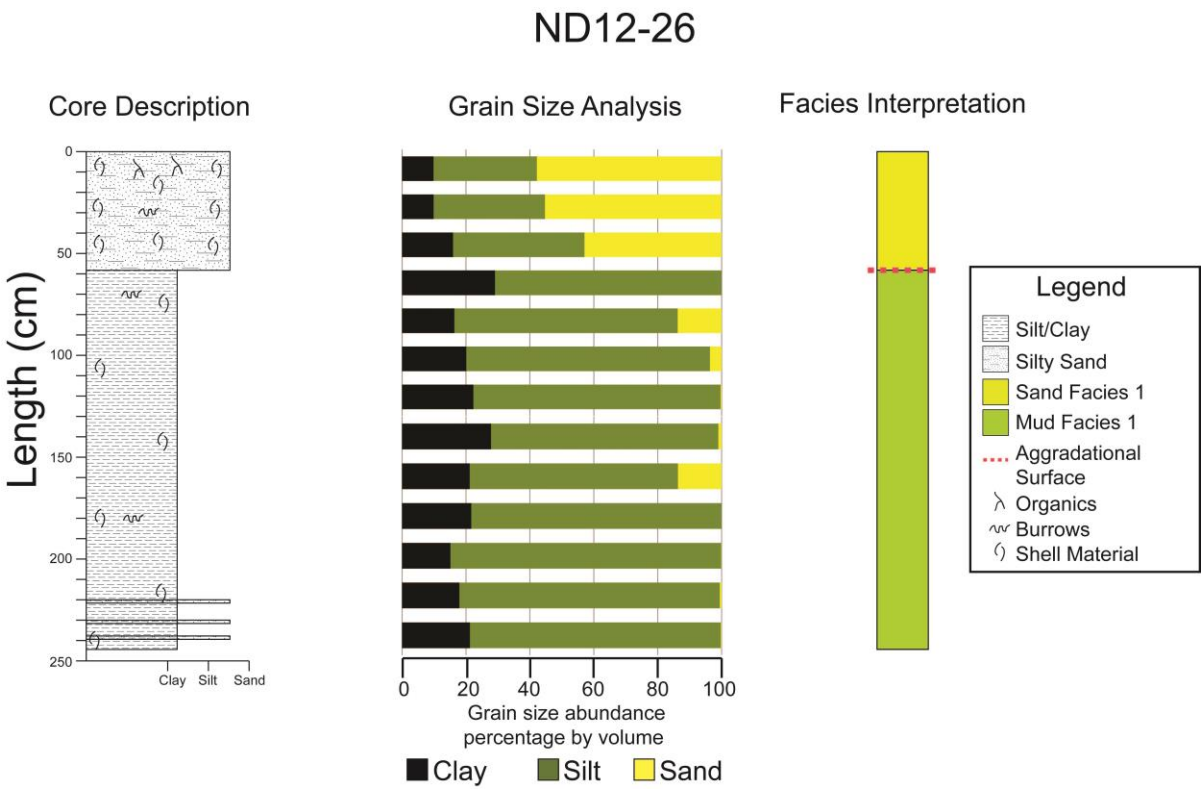

See page 38 for description.

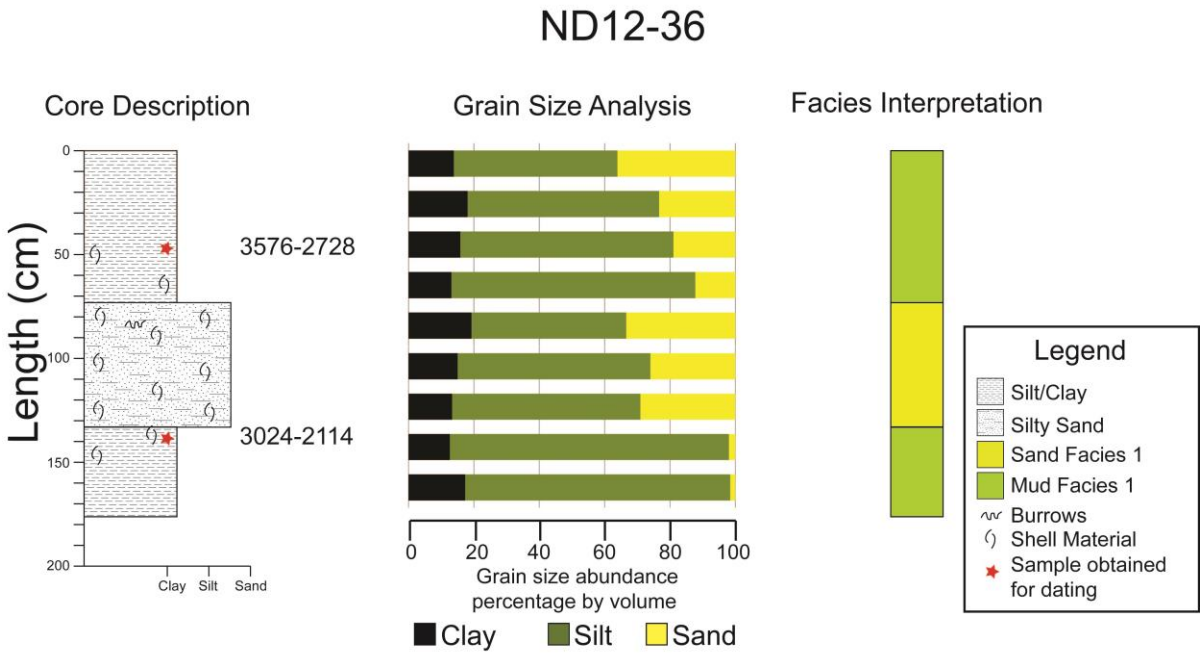

See page 38 for description.

Appendix B

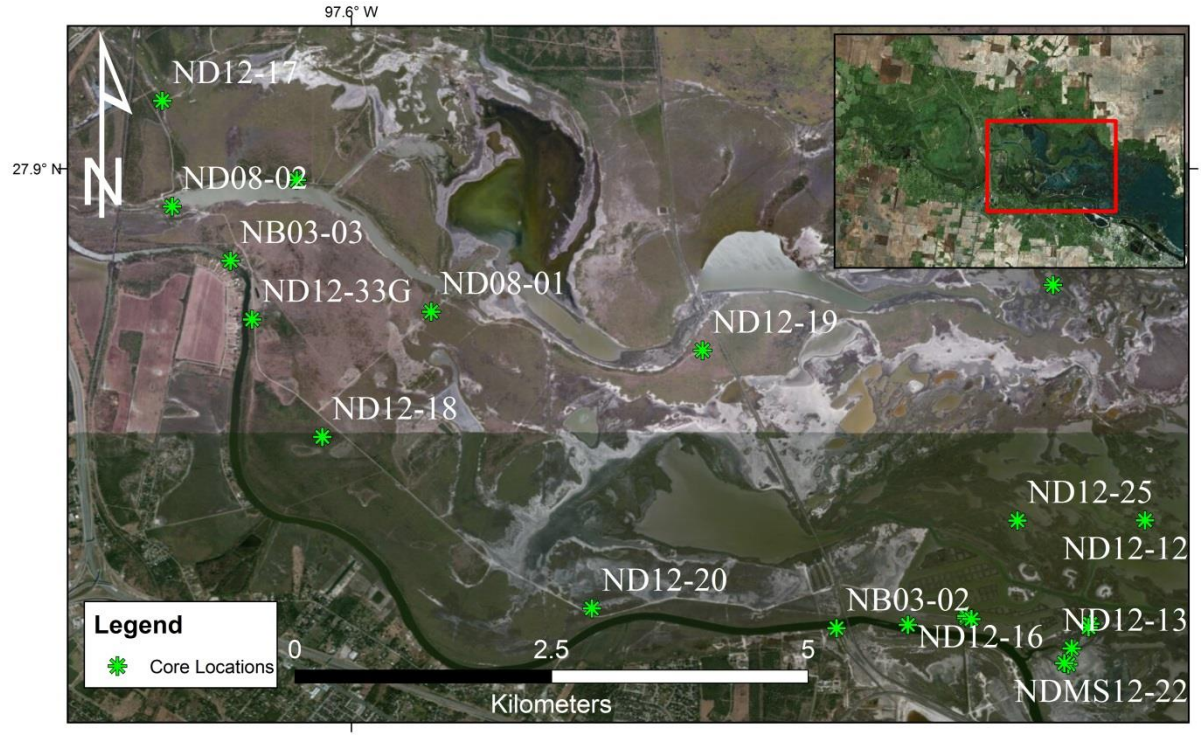

The following four maps show location of all cores. Also shown are the core locations from Simms et al. (2008) are depicted in the maps as well and are denoted with a 'NB' where as cores for this study begin with 'ND'

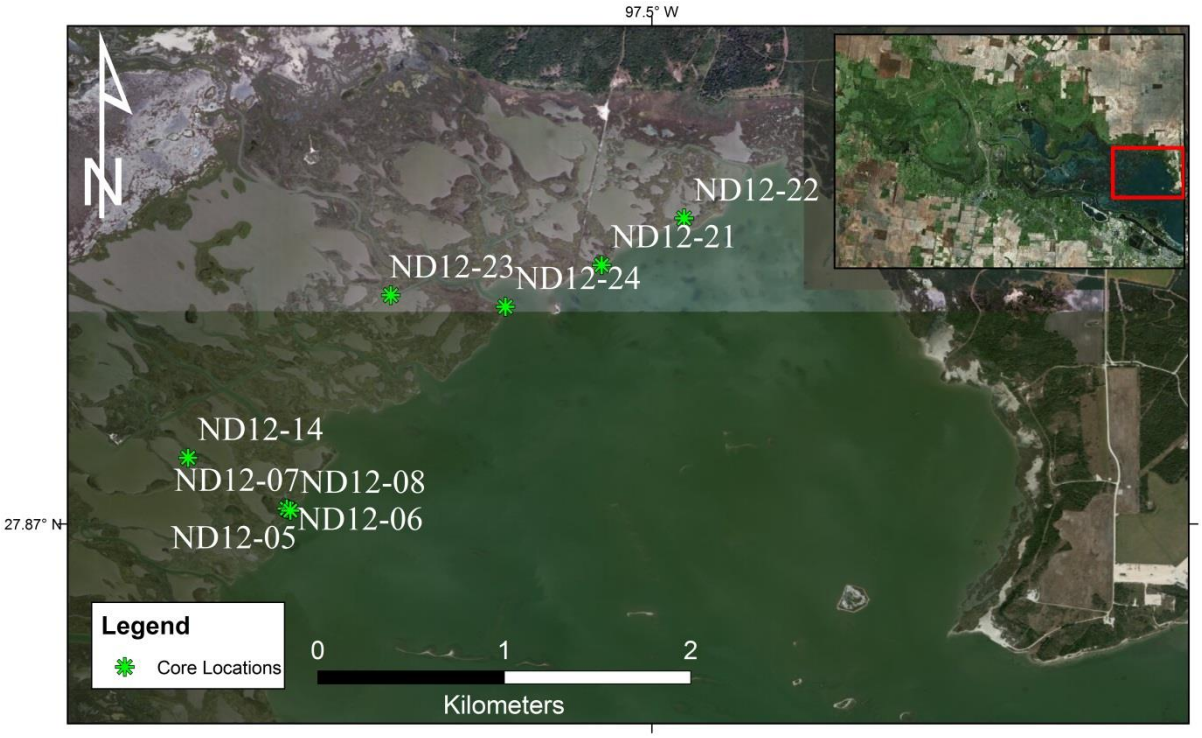

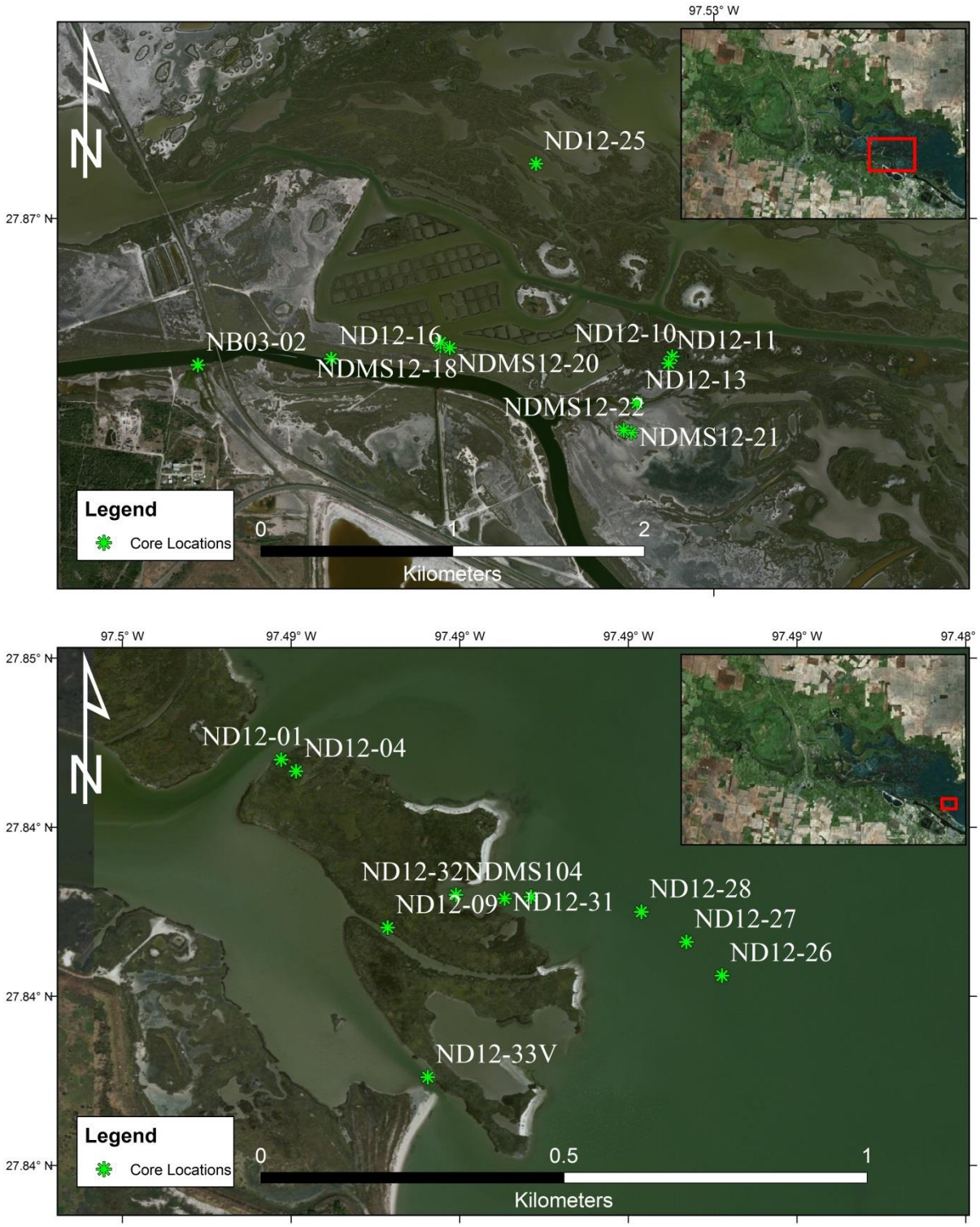
97.53° W
27.87° N
ND12-25
NB03-02
ND12-16
NDMS12-18
NDMS12-20
ND12-10
ND12-11
ND12-13
NDMS12-22
NDMS12-21
Legend
Core Locations
0
1
2
Kilometers
97.5° W
97.49° W
97.49° W
97.49° W
97.49° W
97.48°
27.85° N
27.84° N
27.84° N
27.84° N
ND12-01
ND12-04
ND12-32
NDMS104
ND12-09
ND12-31
ND12-28
ND12-27
ND12-26
ND12-33V
Legend
Core Locations
0
0.5
1
Kilometers

Geoprobes

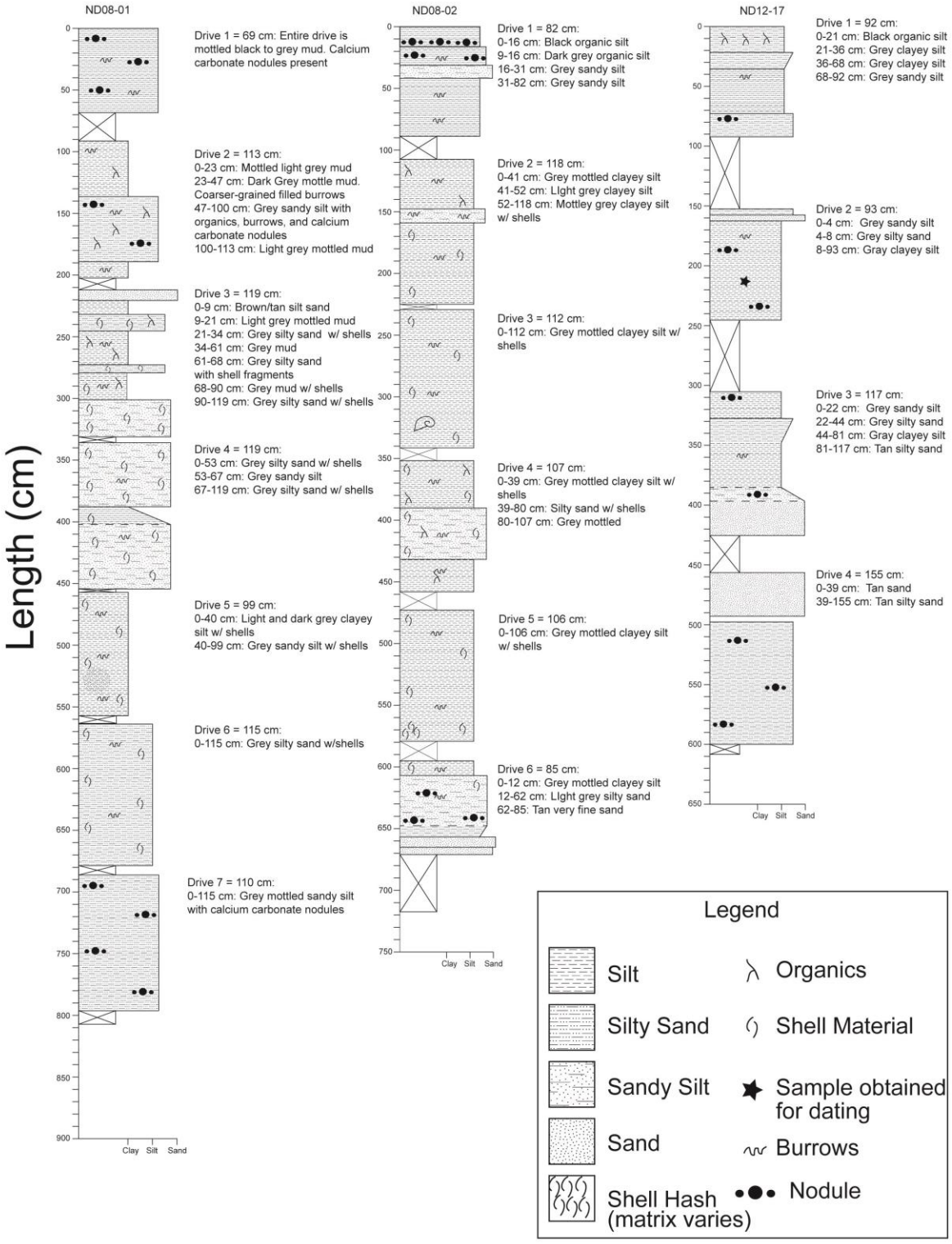

Illustrations of cores used for this study. All scales associated are in centimeters along the y-axis and grain-size along the x-axis.

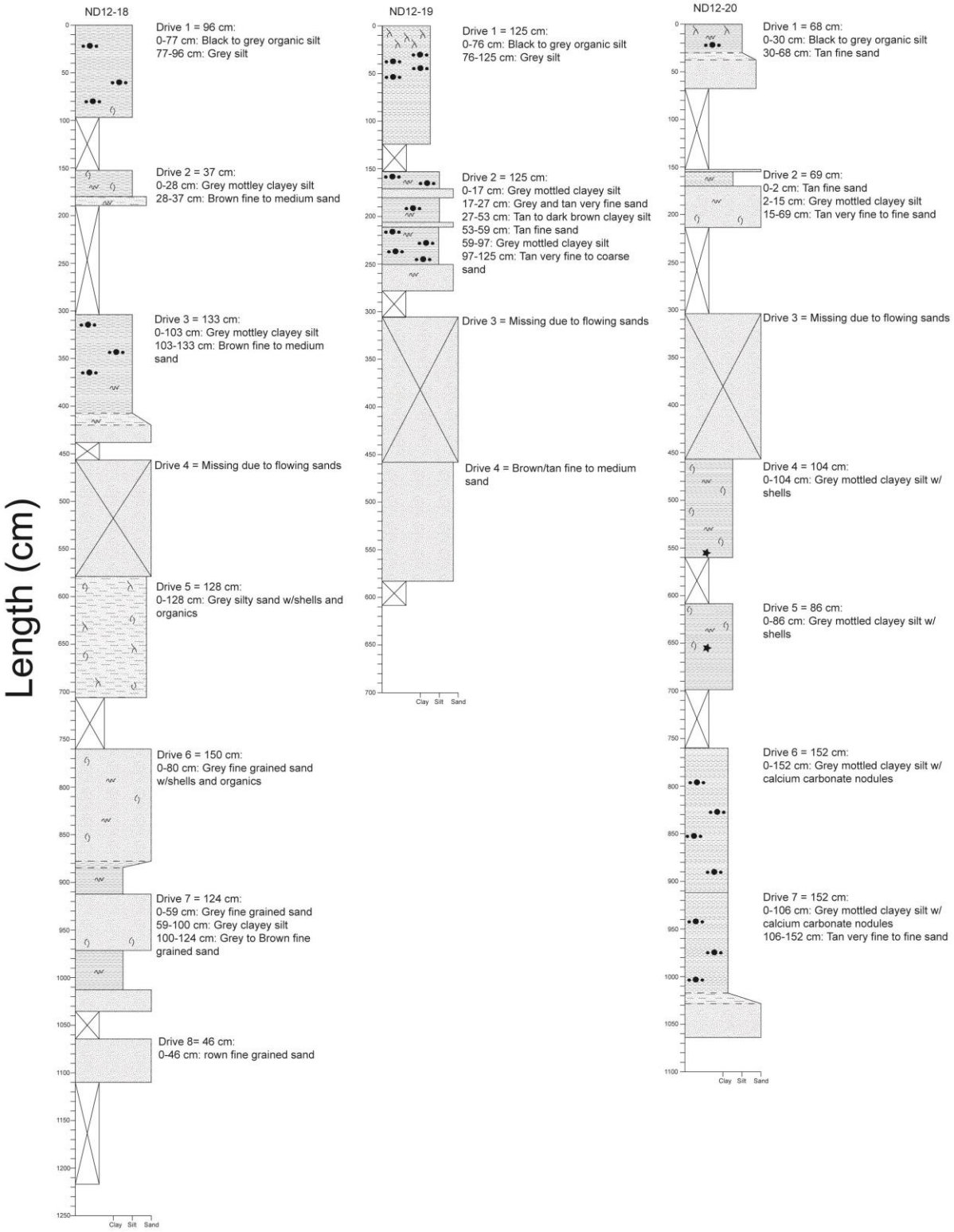

See page 49 for description.

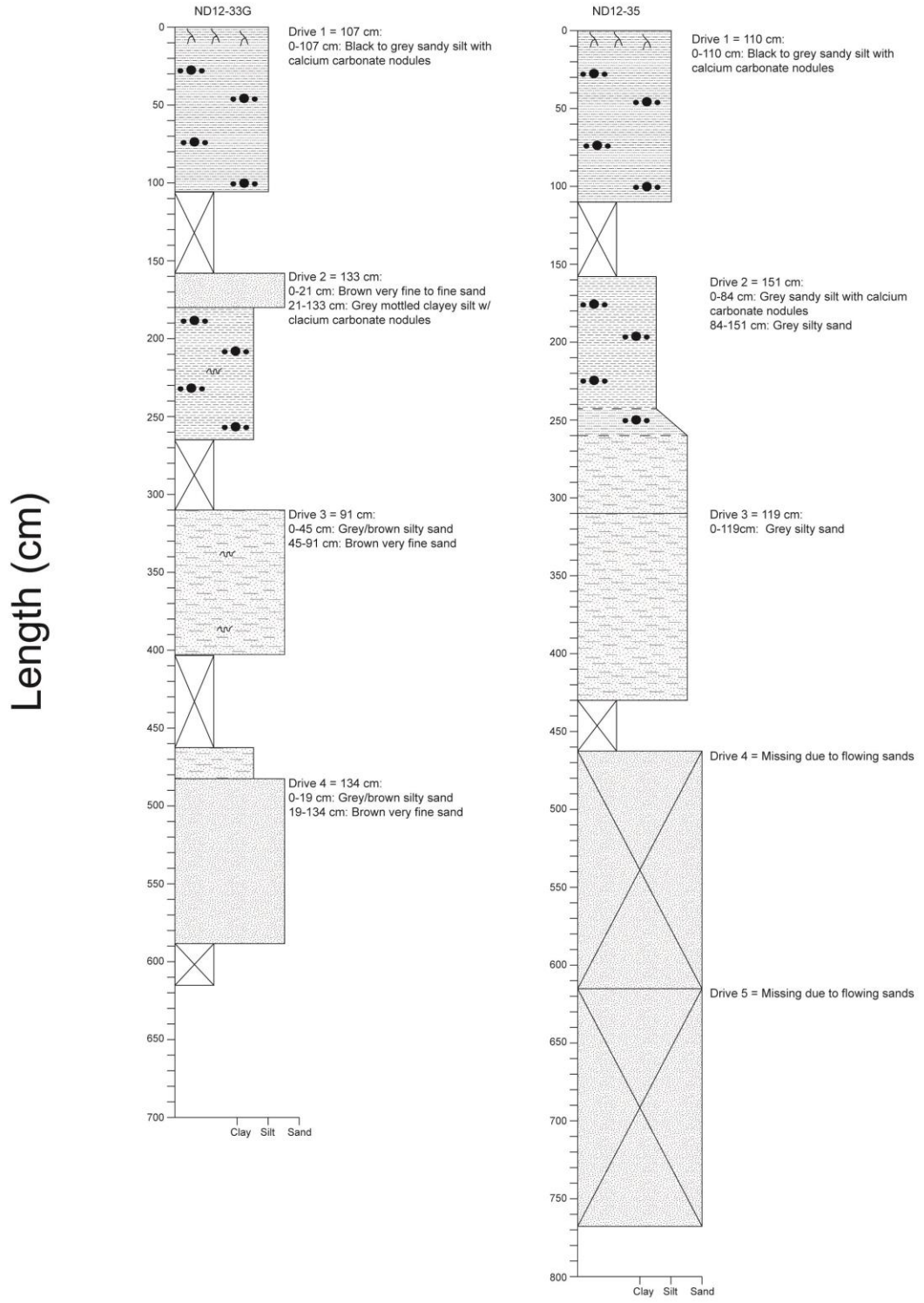

See page 49 for description.

Vibracores

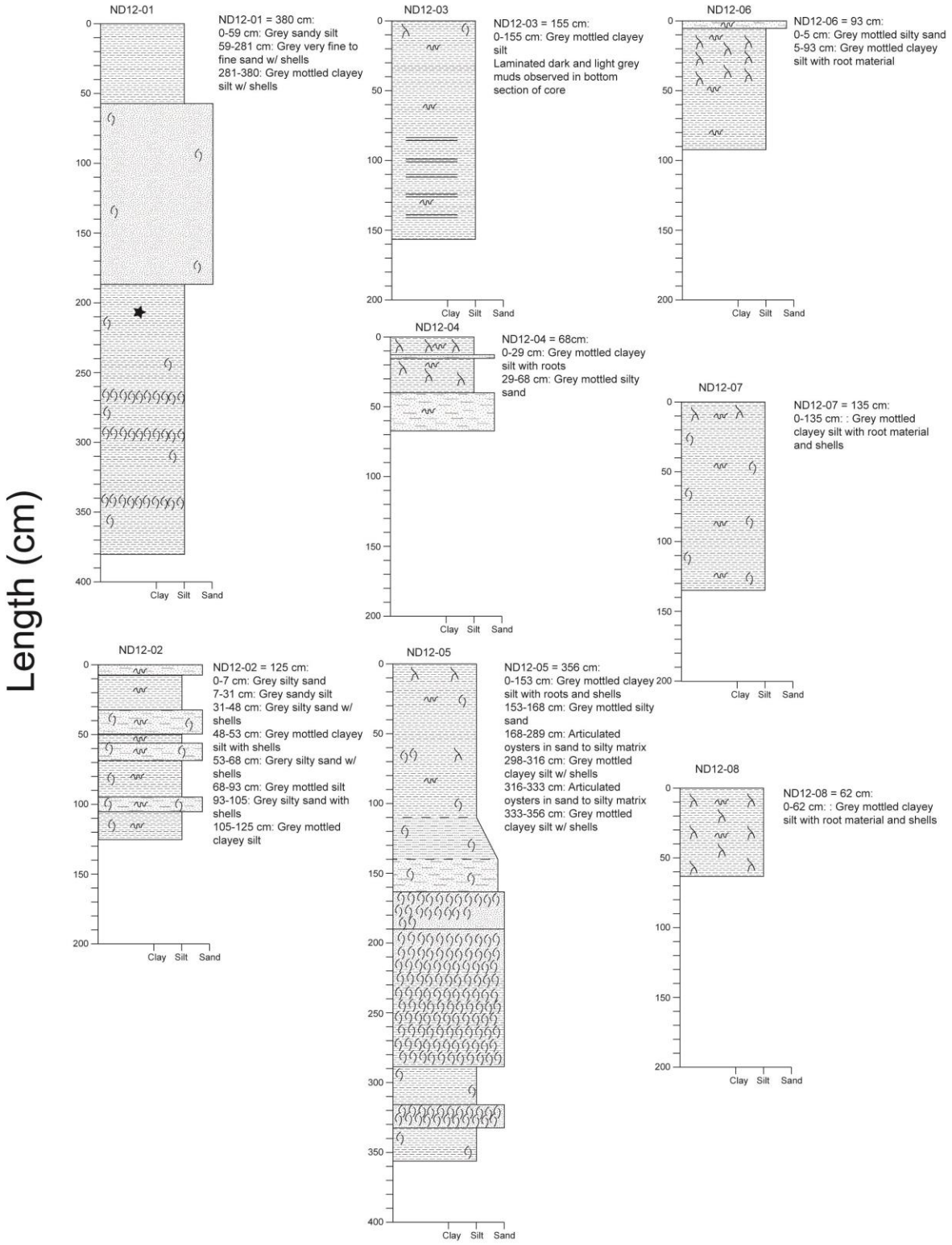

See page 49 for description.

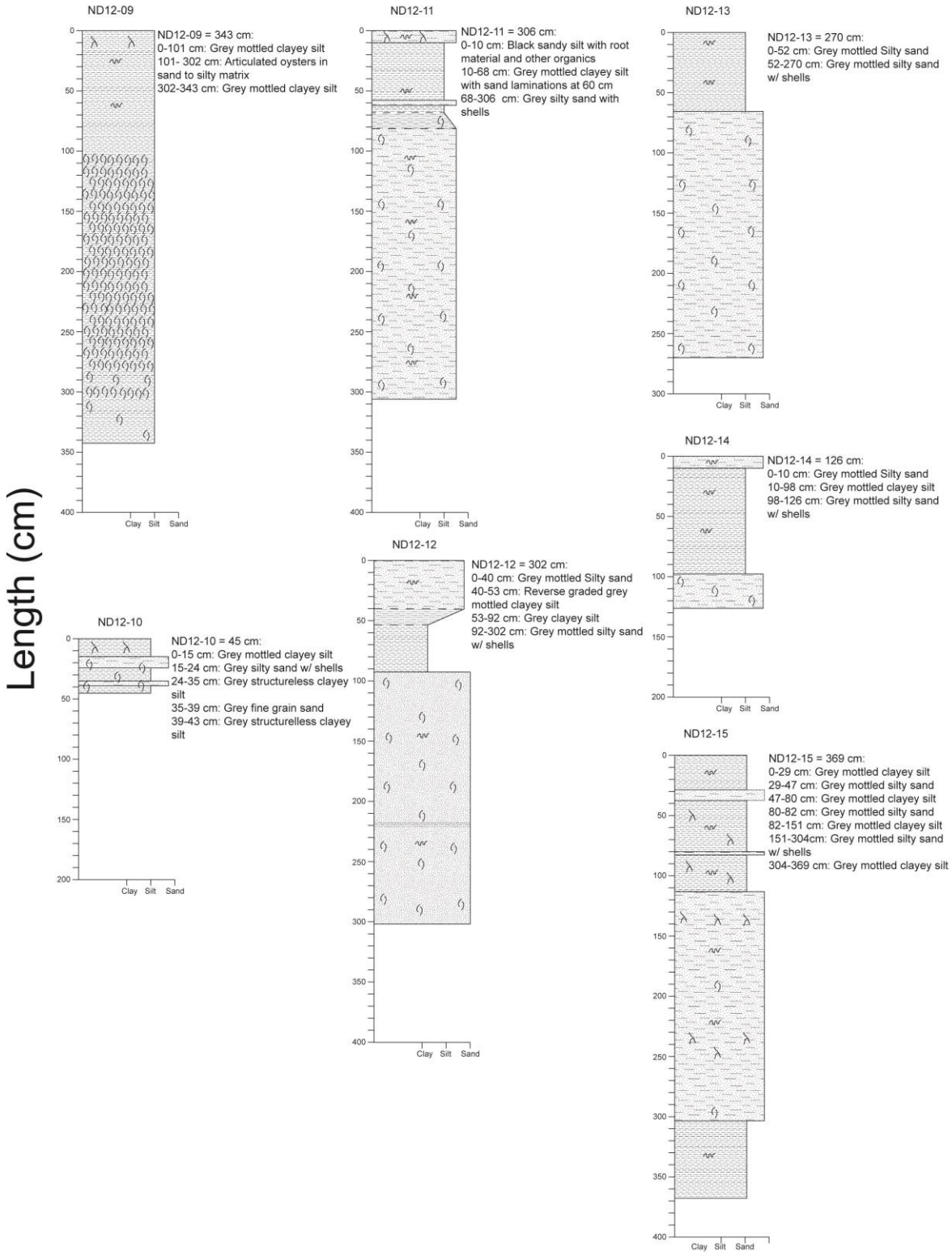

See page 49 for description.

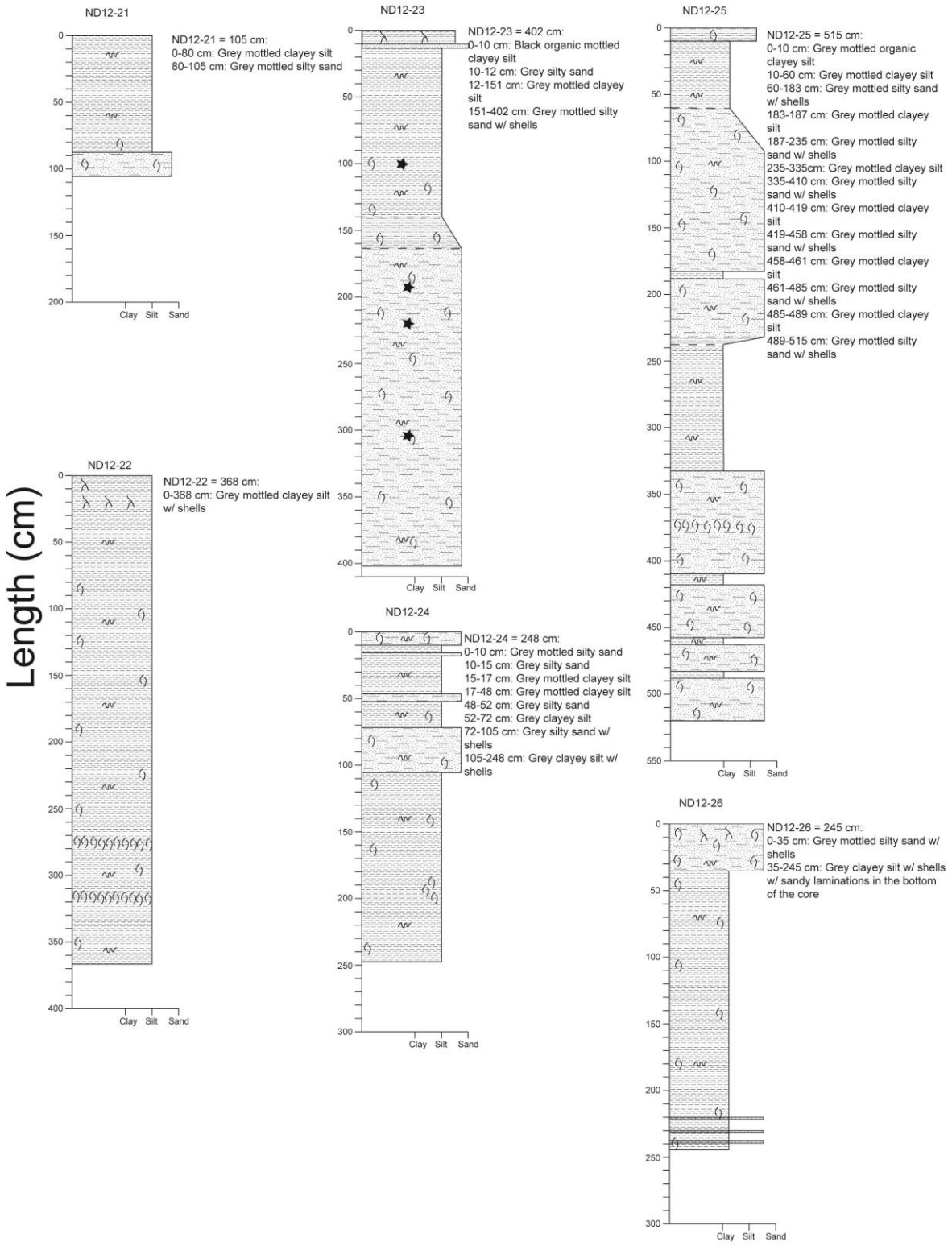

See page 49 for description.

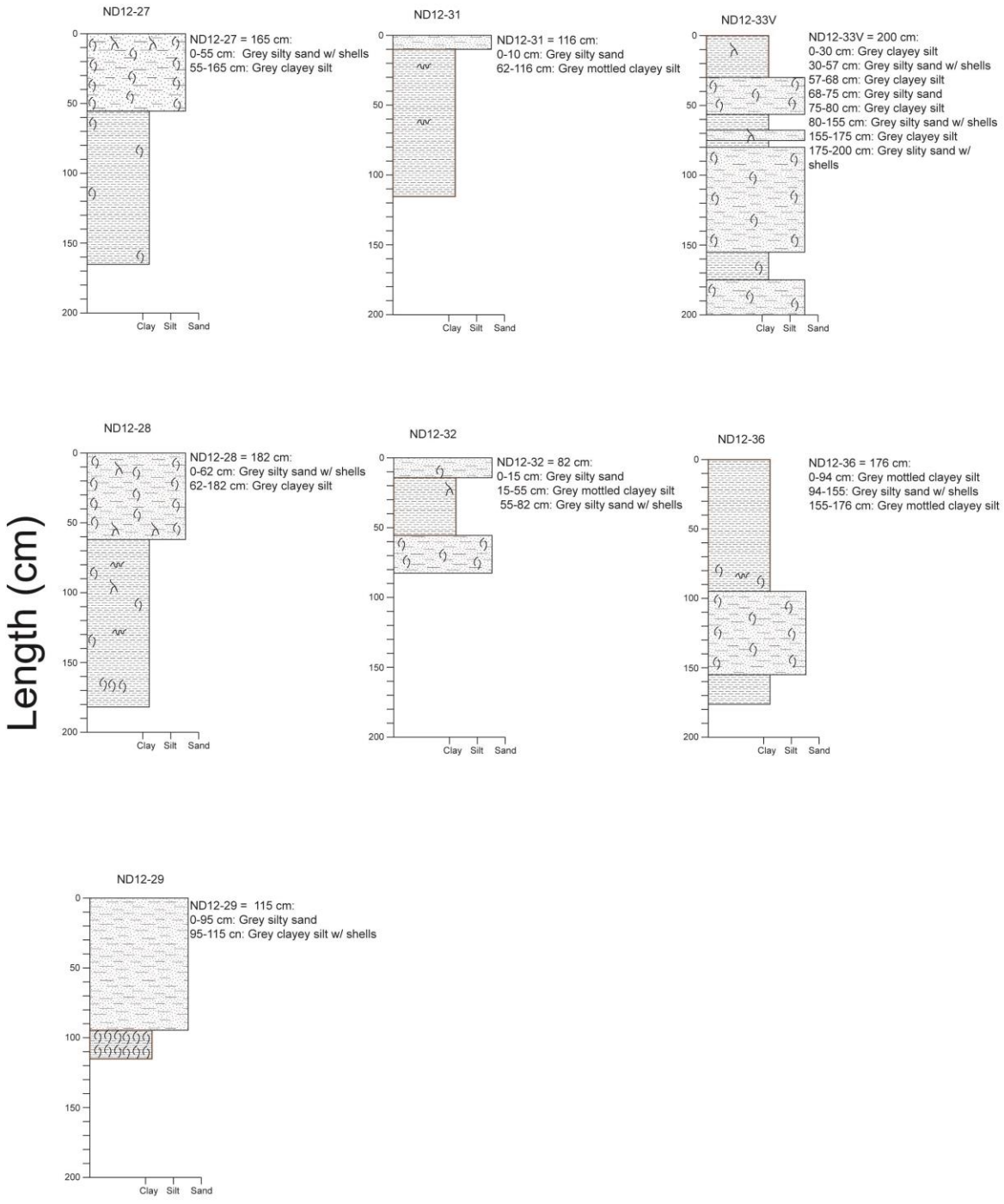

See page 49 for description.